Structures 33 (2021) 4718–4742

Contents lists available at ScienceDirect

Structures

journal homepage: www.elsevier.com/locate/structures

On the distribution of internal forces in single-storey CLT symmetric shear-walls with openings

Daniele Casagrande [a,*], Riccardo Fanti [a], Marco Greco [b], Igor Gavric [c], Andrea Polastri [a]

[a] Institute of Bioeconomy - National Research Council of Italy (CNR-IBE), 38010 San Michele all'Adige, Italy
[b] University of Trento, Department of Civil, Environmental and Mechanical Engineering, Trento, Italy
[c] InnoRenew CoE, 6310 Izola, Slovenia & Faculty of Mathematics, Natural Sciences and Information Technologies, University of Primorska, 6000 Koper, Slovenia

ARTICLE INFO

Keywords:
Cross-laminated timber
Shear-walls
Finite element analysis
Stress distribution
Wood structures
Openings

ABSTRACT

This paper presents a numerical and analytical study on single-storey cross-laminated timber (CLT) shear-walls with openings subjected to lateral loads. The main objective was to investigate the location and distribution of maximum values of axial and shear forces in relevant wall sections. The influence of parameters such as wall geometry (different sizes of wall openings, door openings, lintel/parapet lengths and heights, wall thickness) and different stiffness levels of mechanical anchors for CLT wall connection with floor/foundation were studied. Finite element (FE) parametric analyses were performed on a set of single-storey CLT shear-walls with door and window openings and were compared with analytical models for determination of internal forces. The importance of wall connections' flexibility was identified, as the distribution of internal forces in walls with rigid and flexible anchors were considerably different. The obtained outcomes of this study provide a solid base for the next step, an experimental investigation of in-plane internal force distribution in CLT walls with openings, which will serve for further development of numerical, analytical and design approaches.

1. Introduction

Cross-laminated timber (CLT) as the main structural system has seen exponential growth in the last decade worldwide, and its market share is expected to continue to grow further in the future [5] not only for low-rise, but also mid-rise and high-rise buildings including moderate and high seismic regions due to its good seismic behavior as observed in extensive experimental, analytical and numerical studies [19]. CLT has gained such popularity in construction due to numerous advantages; its low weight and high prefabrication levels reduce transportation and erection cost, enables easy handling and speed of construction, as well as reduces the size of necessary foundations. Further, high strength-to-weight ratio, in addition to a two-way action load transfer possibility similar to reinforced concrete walls and slabs and high in-plane strength and stiffness, makes it a very efficient and desirable construction material. Lastly, one of the most important advantages of CLT is the environmental aspect as it is made of wood, a renewable natural material, which has a much lower carbon footprint compared to other building materials or even negative carbon balance considering its ability to sequester carbon [18].

CLT walls with openings can be fabricated in two different ways, which consequently significantly affect their structural performance. First option is fabrication with fully automated process, where the opening in a CLT wall is done by a CNC machine on a production line. An opening in a CLT wall is typically milled or cut-out from a large full-size panel, forming so called monolithic shear wall. The second option is to join several smaller CLT panels together, typically with self-tapping screws, to form a CLT will with a door or window opening - so called segmented shear-wall [20]. In case of monolithic shear walls, structural continuity between the individual CLT wall segments is achieved through a moment resisting rigid lintel connection (in case of a door opening) or a lintel and parapet connection (in case of a window opening). On the other hand, in segmented CLT shear-wall case, lintels or/and parapets act as partly rigid elements to individual cantilever CLT wall segments, usually not capable of transferring bending moments from one to another CLT wall segment and the structural continuity between the individual lintels/parapets and CLT wall segments is commonly achieved with mechanical screwed connections loaded in shear. These two cases of CLT shear-walls have significantly different strength and stiffness properties, yet it is common in structural design

* Corresponding author.
E-mail addresses: daniele.casagrande@ibe.cnr.it (D. Casagrande), riccardo.fanti@ibe.cnr.it (R. Fanti), marco.greco@studenti.unitn.it (M. Greco), igor.gavric@innorenew.eu (I. Gavric), andrea.polastri@ibe.cnr.it (A. Polastri).

https://doi.org/10.1016/j.istruc.2021.06.084
Received 11 May 2020; Received in revised form 16 May 2021; Accepted 22 June 2021
Available online 26 July 2021

practice to treat both cases in the same way, considering only strength and stiffness of individual cantilever CLT wall element and excluding the contribution of lintels or/and parapets. This is mostly due to non-existing design procedures for determination of internal force levels and distribution in CLT walls with openings subjected to in-plane lateral loads, which can potentially lead to brittle failure modes in the zone between a lintel or a parapet and a CLT wall segment.

The aim of modern seismic design is to dimension structures which will respond in a ductile way during the earthquake, preventing any possibility for brittle failures. To achieve such behaviour the structure should have an adequate capacity to deform beyond its elastic limit without substantial reduction in the overall resistance against horizontal and vertical loads. This design method, also known as capacity design [23], aims to avoid anticipating brittle failures that would prevent the development of a proper ductile global failure mechanism by over-designing the brittle members and forcing the weaker ductile elements to plasticize [6,15]. Application of these principles enhances the designed performance of the entire structure according to performance-based design requirements [30,11].

Bogensperger et al. [3] and Brandner et al. [4] established analytical formulations of in-plane shear strength and stiffness of CLT diaphragms on the material level. Three possible shear failure mechanisms were identified: gross-shear in case of narrow-face bonded laminations, net-shear and torsion failure mode. In the past, several studies were performed on different structural system levels, either on CLT wall elements with window and/or door openings, or on a full scale CLT buildings subjected to lateral loads. Ceccotti et al. [9], Dujic et al. [13] and Popovski et al. [24] performed experimental programme on CLT walls cyclic tests, where some CLT shear-walls were with door and/or window openings. Performance of shear-walls with openings exhibited comparable strength capacities to shear-walls without openings due to failure mechanisms predominantly concentrated in mechanical anchoring connections (hold-downs and angle brackets), while a decrease in wall stiffness was observed. Dujic et al. [12,13] further focused on analytical description of strength and stiffness reduction of CLT walls with openings related to the openings' aspect ratios, supported by numerical non-linear static pushover models. They proposed a simplified procedure for calculation of global reduction in stiffness and strength of CLT walls with large openings. Awad et al. [1] performed experimental investigation of CLT walls with openings with additional analytical models for estimation of overall wall strength, and numerical models for estimation of global elastic behaviour and prediction of failure mechanism of CLT panels with openings subjected to lateral loads. Further, Shahnewaz et al. [26] performed a numerical study including sensitivity analysis of different parameters and proposed refined analytical expressions for estimation of in-plane CLT wall stiffness, considering influences of different sizes and shapes of the openings and the aspect ratios of the openings, as well as the wall aspect ratios. Pai et al. [22] studied force transfer around openings in CLT shear-walls in terms of the effect given by the openings on the global force–deformation response of the CLT wall. Cases with cut-out openings and assembled panels with screws and additional force transfer tie-rod straps were numerically modeled and the influence of anchoring layout on design transfer forces around openings were identified. Mestar et al. [20] proposed equivalent-frame model applicable to CLT shear-walls with openings. While reasonable fit was observed in terms of global elastic stiffness, prediction of internal forces was not reliable in all cases. The kinematic modes of CLT shear-walls with cut-out openings were studied through numerical analyses and full-scale tests on single-storey CLT shear-wall with either door or window opening by Mestar et al. [21], showing that lintel's slenderness and hold-down flexibility greatly affect on the global behaviour.

On a structural system level of an entire building, Popovski and Gavric [25] studied experimental performance of CLT walls with large openings within a full scale 2-storey CLT building subjected to quasi-static monotonic and cyclic loading. Brittle local failure of a CLT wall panel was observed in the area of the upper corner of a large door opening. Sustersic et al. [27] performed parametric FE investigation on a CLT case study building, exposing the importance of proper assessment of stress distribution around CLT walls with openings and providing sufficient overstrength in order to avoid brittle failure modes according to capacity design principles of CLT buildings. Therefore, to avoid such undesirable brittle failures, more information and knowledge about internal force levels and their distribution around the openings in CLT walls is crucial for the development of reliable design approaches which would enable proper estimation of stress levels in critical CLT wall sections to avoid potential undesirable failure mechanisms.

In this paper, a numerical and analytical study on distribution of in-plane internal axial and shear forces in single storey monolithic CLT shear-walls with cut out openings is presented. The main goal of the study is to identify critical zones of maximum axial and shear forces due to in-plane lateral loading of CLT shear-wall with openings, and to predict levels of internal forces for further development of design methods for CLT walls with openings subjected to in-plane lateral loads. Several parameters may influence the distribution and levels of internal forces in CLT shear-walls, such as: geometrical properties of door and window openings (length of wall segments, height and lengths of lintels and parapets, etc.), orthotropic nature of CLT as a structural material, specific type of discrete connection of shear-walls to slabs below them or to foundation by means of mechanical connectors (i.e. hold-downs and angle brackets), whose flexibility may have a significant influence on the internal distribution of stresses in the panel. Parametric numerical finite element (FE) analyses are carried out to investigate the influence of abovementioned parameters. Further, analytical predictions and mechanical models are proposed to predict the axial and shear stresses in wall segments and lintels, the maximum values of shear and axial stresses are determined and compared.

Despite different levels of vertical loads [17] and contribution of diaphragm effect of slabs in multi-storey CLT buildings [28] may also influence the distribution and levels of internal forces in CLT shear-walls due to their influence on kinematic modes of CLT walls, these parameters related to multi-storey effects are out of scope of the study presented in this paper and will be subjects of continuing steps of this research topic. Therefore, in this first step the research investigation, mainly focuses on properly analytical addressing of internal forces distribution in single-storey CLT symmetric shear-walls with openings subjected only to lateral loads such as seismic or wind loads.

The main objectives of this study are:

i) to investigate the location of the maximum values of the internal forces per unit length and the influence of parameters on the distribution of internal forces, such as wall geometry (different sizes of wall openings, door openings, lintel/parapet lengths and heights, wall thickness) and different stiffness levels of mechanical anchors for CLT wall connection with foundation;
ii) to predict analytically the distribution of shear and axial forces per unit length in the relevant sections of single-storey CLT shear-walls with openings subjected to lateral loads.

It is worth noting that the results are shown in terms of forces per unit length and not in terms of stresses which can be determined by taking into account the layup of the panels.

2. Finite element analysis for the study of internal forces

The study of the internal forces distribution in CLT shear-walls with openings is carried out by means of Finite Element (FE) analyses implemented in the software package SAP2000 [10]. The influence of the geometrical dimensions and the stiffness of the mechanical anchors is investigated via a parametric analysis. Both door and window openings are considered in the study. Specific attention is paid to the difference for the location of maximum internal forces between rigid (R) and flexible (F) anchor systems of the shear walls.

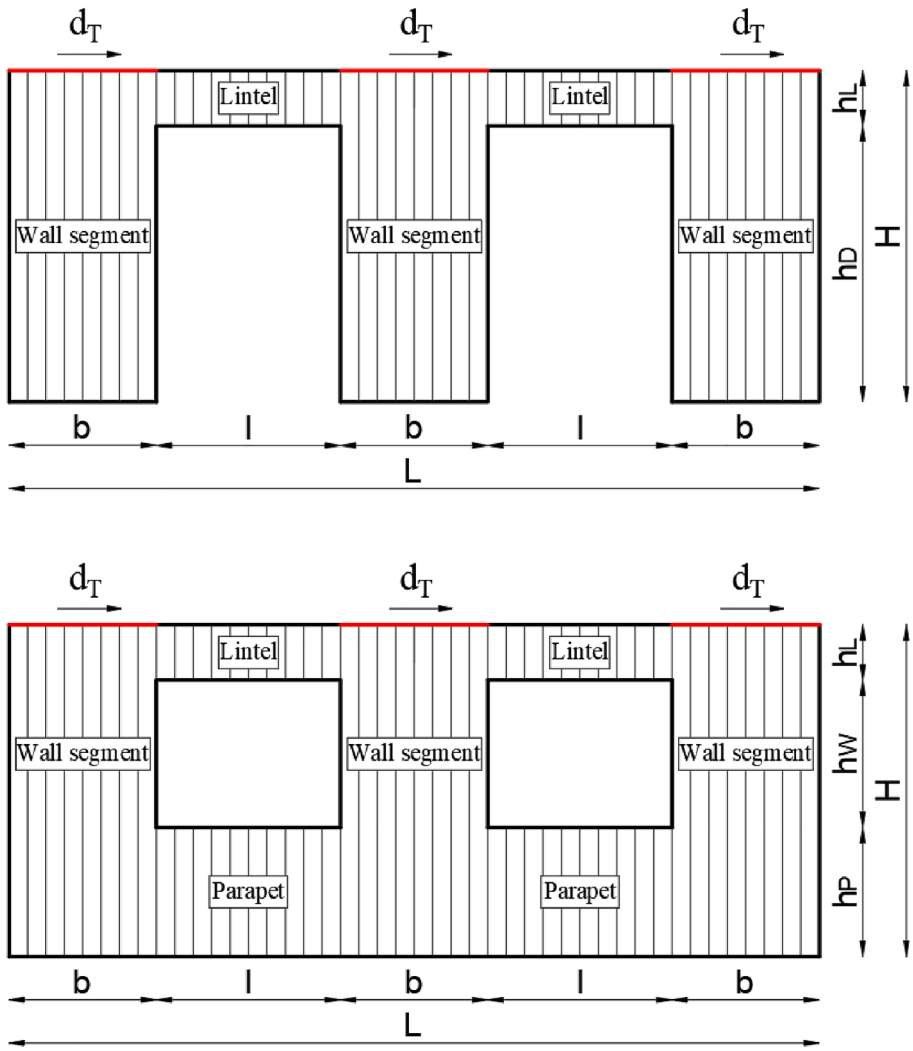

Fig. 1. Geometrical properties of CLT shear-walls with door and window openings.

Table 1
Geometrical values adopted in the parametric analysis.

wall segment's width	*b [m]*	1.20	1.80	2.40
lintel length	*l [m]*	0.90	1.50	2.10
lintel height	h_L *[m]*	0.30	0.45	0.75

2.1. Case studies

Symmetric CLT shear-walls with either two identical door or two window openings are adopted as case studies in the FE analyses, see Fig. 1. Each shear-wall is characterized by three identical wall segments and two identical lintels. The geometrical dimensions of case studies were selected based on practical sizes used in CLT constructions.

A height H equal to 2.70 m was taken for all configurations. Three values of the vertical wall segment's width (b) were adopted namely [1.20; 1.80; 2.40] m. The lintel length (l) and height (h_L) were analysed for values of [0.90; 1.50; 2.10] m and [0.30; 0.45; 0.75] m, respectively, see Table 1. A height of the parapet (h_P) equal to 1.05 m was adopted for all configuration with window openings. Two different CLT panel layups, namely a 100 mm thick 5-layer (20z-20x-20z-20x-20z) and a 160 mm thick 5-layer (30z-35x-30z-35x-30z) were selected for the analyses. The outer boards in the CLT panels were assumed to be parallel to the vertical direction. A board width equal to 0.15 m was taken for all case studies. The modulus of elasticity of boards parallel and perpendicular to grain, E_0 is equal to 12000 MPa [14]. The value of the in-plane shear modulus G_0 is assumed equal to 690 MPa [14], respectively.

Each wall segment was anchored to the foundation by means of one hold-down in each corner and a number n_a of angle brackets proportional to the wall segment's width b, see Table 2. In case of flexible anchor system, an uniaxial behaviour along the vertical direction was

Table 2
Stiffness values of mechanical anchors.

Mechanical Anchor	Number per wall segment [-]		Tensile stiffness (z-direction) [kN/m]	Shear stiffness (x-direction) [kN/m]
Hold-down	1 per each corner		$k_{h,z,t} = 6609;13247$	-
Angle brackets	$n_a = 2$	$b = 1.20\ m$	$k_{a,z,t} = 2530$	$k_{a,x} = 2090$
	$n_a = 3$	$b = 1.80\ m$		
	$n_a = 4$	$b = 2.40\ m$		

Table 3
Values of equivalent modulus of elasticity and shear modulus for CLT panels.

t	Layup	t_x	t_z	$E_{eq,x}$	$E_{eq,z}$	G_{eq}
[mm]		[mm]	[mm]	[MPa]	[MPa]	[MPa]
100	20z-20x-20z-20x-20z	40	60	4800	7200	563
160	30z-35x-30z-35x-30z	70	90	5250	6750	494

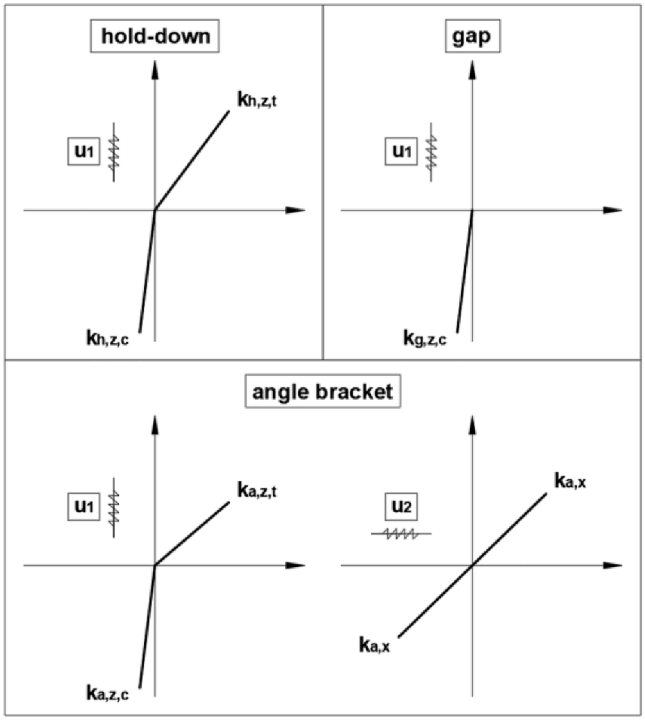

Fig. 2. Force–displacement graph for hold-down, angle brackets and gap elements.

assumed for the hold-downs: only the tensile stiffness is considered while the horizontal (shear) stiffness is neglected, as demonstrated by Gavric et al. [16]. Two values of the hold-down tensile stiffness $k_{h,z,t}$, reported in Casagrande et al. [7] were considered namely equal to 6609 kN/m and 13247 kN/m for WHT 440 and WHT620 hold-down with 30 and 55 4x60 mm nails, respectively. Conversely, a biaxial behaviour of the angle brackets was considered; a shear horizontal $k_{a,x}$ and tensile vertical $k_{a,z,t}$ stiffness equal to 2090 kN/m and 2530 kN/m was taken according to Gavric et al. [16]. In case of rigid anchor system (R) the base of wall segments and the bottom edge of parapets were assumed to be rigidly connected to the ground.

A total of 27 geometrical configurations with 2 different wall thicknesses and 2 values of the hold-down tensile stiffness, in addition to rigid anchor system, were analysed, yielding a total of 162 cases for each wall opening type (window or door) case study.

2.2. FE modelling

Elastic four-joints quadrilateral homogenous shell elements available in the SAP 2000 software [10] were used to model the shear-walls with the same thickness of the CLT panel. A mesh size of 37.5 mm × 37.5 mm was chosen based on the mesh refinement analysis reported in Appendix A1. An orthotropic material was assigned to the shell elements by defining the equivalent values of the modulus of elasticity for horizontal $E_{eq,x}$ and vertical $E_{eq,z}$ directions were determined from Eqs. (1) and (2) as reported in Mestar et al. [20]:

$$E_{eq,x} = \frac{E_0 \bullet t_x}{t} \quad \text{along the x} - \text{horizontal direction} \tag{1}$$

$$E_{eq,z} = \frac{E_0 \bullet t_z}{t} \quad \text{along the z} - \text{vertical direction} \tag{2}$$

where t_z, t_x are the total thickness of the vertical and horizontal layers, respectively, t is the total thickness of the CLT panel. An equivalent shear modulus G_{eq} was determined according to the method proposed by Brandner et al. [4] taking into account both shear and torsional deformation contribution of laminations according to Eq. (3):

$$G_{eq} = \frac{G_0}{1 + 6 \bullet \alpha_T \bullet} \left(\frac{t_{mean}}{a}\right)^2 \tag{3}$$

where G_0 is the shear modulus of the laminations, a is the width of laminations, t_{mean} is the mean thickness of laminations, see Eq. (4), and α_T is obtained from Eq. (5).

$$t_{mean} = \frac{t_{tot}}{N} \tag{4}$$

$$\alpha_T = p \bullet \left(\frac{\mathrm{t_{mean}}}{\mathrm{a}}\right)^{\mathrm{q}} \tag{5}$$

where N is the number of layers, q is equal to −0.79 and p is equal to 0.53 and 0.43 for 3 and 5 layers of the CLT panel, respectively. A null value of the Poisson's ratio was assigned as suggested by Berg et al. [2]. Table 3 provides the values of $E_{eq,x}$, $E_{eq,z}$ and G_{eq} adopted for the two CLT panel layups adopted in the analyses.

For the analyses with flexible anchor system, each hold-down was modelled with a 1-direction elastic multi-linear link with a tensile stiffness equal to $k_{h,z,t}$ and a value of the compressive stiffness equal to $k_{h,z,c}$ which simulates the contact of the CLT panel with the foundation, see Fig. 2. The angle brackets were modelled by means of 2-direction multi-linear links. A linear behaviour was selected for the horizontal direction with a value of stiffness equal to $k_{a,x}$. As for the hold-down, an elastic multi-linear behaviour was adopted along the vertical direction with a tensile stiffness equal to $k_{a,z,t}$ and a compressive stiffness equal to $k_{a,z,c}$. Vertical gap elements were located along the entire base of the wall segments for the joints not directly connected to the ground by means of any mechanical anchor. The compressive stiffness of hold-down $k_{h,z,c}$, angle brackets $k_{a,z,c}$ and gaps $k_{g,z,c}$ along the vertical directions was equal to 10^6 kN/m in order to simulate a rigid contact of the shear-wall with the ground. For the analyses with rigid anchor system, the horizontal and vertical displacements of all the joints along the base of the wall segments were prevented by simple-pinned restraints.

Due to the non-linearity of hold-down and angle brackets along the z-vertical direction, elastic non-linear analyses were carried out. A lateral displacement d_t was imposed to all the joints on top of the wall segments. It is worth noting that, however, the results in terms of distribution of internal forces are not influenced by the amplitude of the imposed lateral displacement since the vertical load was not considered in this study but will be covered in the next phase of this research investigation. A linear relationship between the displacement imposed and the internal stresses can be in fact established. Future analyses will be carried out with the aim to study the influence of vertical load in the internal stress distribution of CLT shear-wall with openings and the variations due to the amplitude of the imposed lateral load.

3. Location of the maximum values of axial and shear in-plane forces

3.1. Description of the analysis method

The location of the maximum values of axial n and shear v in-plane forces per unit length is investigated. The values of shear forces per

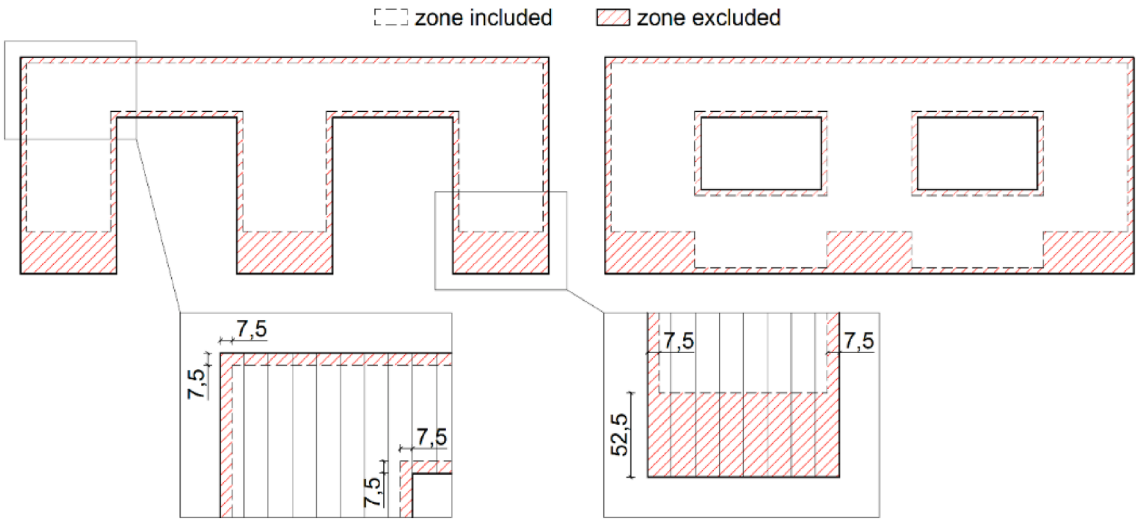

Fig. 3. Zones included/excluded for the determination of maximum values in FE analyses. Values in [cm].

unit length v are directly obtained from the analysis whereas the values in terms of axial in-plane forces n are determined by taking into account the total thickness of boards along x- and z-direction as reported in Eq. (6):

$$n = \begin{cases} n_x & if \quad \frac{n_x}{t_x} \geq \frac{n_z}{t_z} \\ n_z & if \quad \frac{n_x}{t_x} < \frac{n_z}{t_z} \end{cases} \tag{6}$$

where n_x and n_z are the axial in-plane forces per unit length along the x and z directions taken from the analyses.

The location of maximum in-plane forces per unit length was determined by excluding the joints along the edges of the panels and the bottom of columns, as shown in Fig. 3, where the influence of base connections and numerical issues may cause unrealistic values of forces. The exclusion zone analysis is presented in Appendix A2.

3.2. Location of the maximum values for shear-walls with door openings

The location of maximum values of internal forces per unit length are reported in Table 4 for 100 mm thick CLT shear-walls with door openings for a height h_L and a length of lintels l equal to [0.30; 0.75]m and [0.90; 2.10]m, respectively. It is worth noting that the maximum values of internal forces reported in the Figs. 4 and 8 are specific for the displacement loaded direction.

As shown in Fig. 4, the location of the maximum values of the axial internal forces can be located either at the Base-sections of Wall Segments (B-WS) or at the End-sections of Lintels (E-L) whereas the maximum values of shear internal forces are observed either in the centre of the Mid-section of Wall Segments (M-WS), in the centre of the Mid-section of Lintels (M-L) or in the top Corners of the Door Openings (C-DO).

No differences in the locations of maximum values were detected between 100 mm and 160 mm thick walls. As reported in Table 4, the same locations of maximum values were obtained for the cases with flexible hold-downs. Significant differences were conversely observed between walls with rigid and flexible anchors.

The maximum values of axial forces in walls with rigid anchors are located at the Base-section of Wall Segments (B-WS) whereas, in case of flexible anchors, the maximum values move to the End-section of Lintels (E-L) for all analysed cases. The distribution of axial internal forces in the lintel and in the wall segments is shown in Fig. 5 for $b = 1.20$ m, $h_L = 0.30$ m, $l = 2.10$ m.

The maximum values of the shear forces in walls with rigid anchors are located in the centre of the mid sections of wall segments (M-WS) for lintel's length equal to 2.10 m, see Fig. 6a. Conversely, when the lintel's length is equal to 0.90 m the maximum values are located in in the centre of mid sections of lintels (M-L). The only exception is represented by the case with $b = 2.40$ m, $h_L = 0.30$ m, $l = 0.90$ m where the

Table 4
Locations of maximum values of internal forces for walls with door openings - t = 100 mm.

			Rigid		Flexible			
t = 100 mm			[-]		$k_{h,z,t}$ = 6609 kN/m		$k_{h,z,t}$ = 13247 kN/m	
b [m]	h_L [m]	l [m]	Axial	Shear	Axial	Shear	Axial	Shear
1.20	0.30	2.10	B-WS (1 to 6)	M-WS (1 to 3)	E-L (2 to 4)	C-DO (1, 4)	E-L (2 to 4)	C-DO C-DO (1, 4)
1.20	0.30	0.90	B-WS (1, 6)	M-L (1, 2)	E-L (2, 3, 5)	M-L (1, 2)	E-L (2, 3, 5)	M-L (1, 2)
1.20	0.75	2.10	B-WS (1, 6)	M-WS (2)	E-L (5)	C-DO (1, 4)	E-L (5)	C-DO (1, 4)
1.20	0.75	0.90	B-WS (1, 6)	M-L (1, 2) C-DO (1 to 4)	E-L(5)	M-L (1, 2) C-DO (1, 4)	E-L(5)	M-L (1, 2) C-DO (1, 4)
1.80	0.30	2.10	B-WS (1 to 6)	M-WS (1 to 3)	E-L (1 to 4)	C-DO (1, 4)	E-L (1 to 4)	C-DO (1, 4)
1.80	0.30	0.90	B-WS (1, 6)	M-L (1, 2) M-WS (1 to 3)	E-L (2, 3, 5)	M-L (1, 2)	E-L (2, 3, 5)	M-L (1, 2)
1.80	0.75	2.10	B-WS (1, 6)	M-WS (2)	E-L (5)	C-DO (1, 4)	E-L (5)	C-DO (1, 4)
1.80	0.75	0.90	B-WS (1, 6)	M-L (1, 2) C-DO (1, 4)	E-L(5)	M-L (2) C-DO (1, 3, 4)	E-L(5)	C-DO (1, 4)
2.40	0.30	2.10	B-WS (1 to 6)	M-WS (1 to 3)	E-L (1 to 4)	C-DO (1, 4)	E-L (1 to 4)	C-DO (1, 3, 4)
2.40	0.30	0.90	B-WS (1, 6)	M-WS (1 to 3)	E-L (2, 3, 5)	M-L (1, 2)	E-L (2, 3, 5)	M-L (1, 2)
2.40	0.75	2.10	B-WS (1, 6)	M-WS (1 to 3)	E-L (5)	C-DO (1)	E-L (5)	C-DO (1, 4)
2.40	0.75	0.90	B-WS (1, 6)	M-L (1, 2)	E-L (5)	M-L (2) C-DO (1)	E-L (5)	C-DO (1)

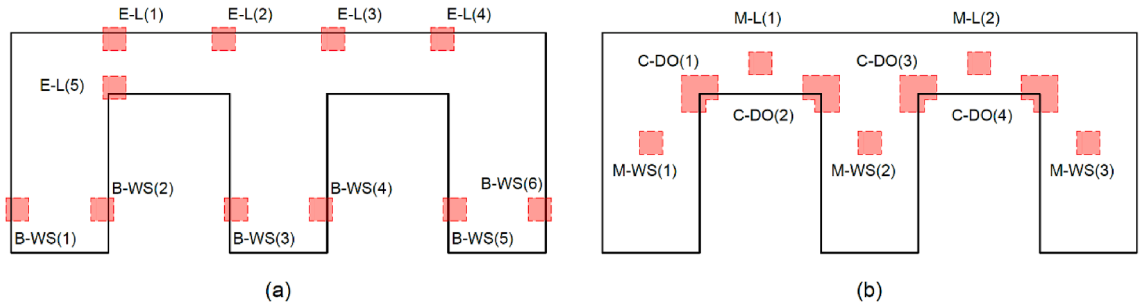

Fig. 4. Legend of locations for maximum values of internal (a) axial and (b) shear forces for shear-walls with door openings.

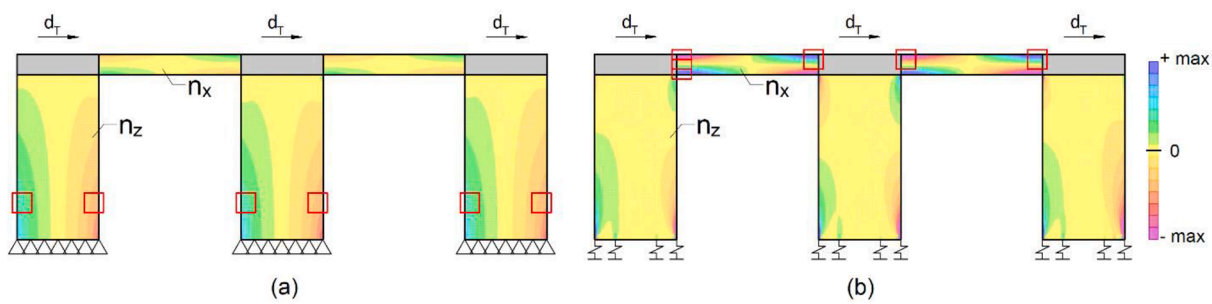

Fig. 5. Axial forces in wall segments and lintels with (a) rigid and (b) flexible anchors - t = 100 mm, b = 1.20 m, h_L = 0.30 m, l = 2.10 m.

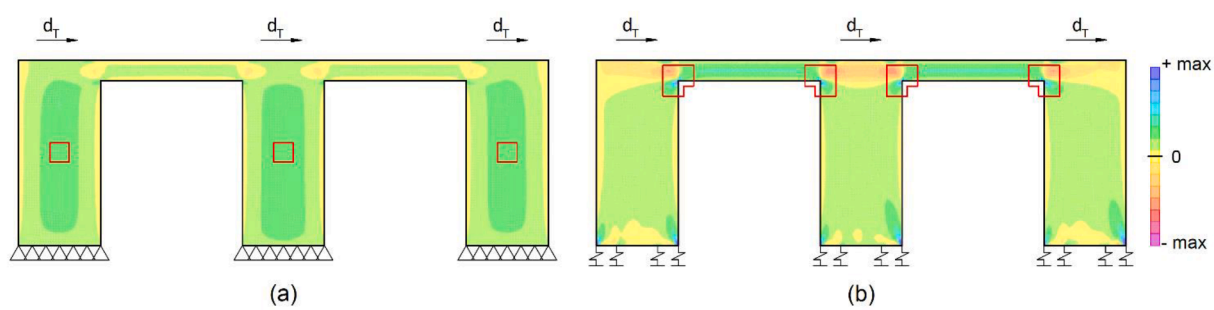

Fig. 6. Shear forces with (a) rigid and (b) flexible anchors - t = 100 mm, b = 1.20 m, h_L = 0.30 m, l = 2.10 m.

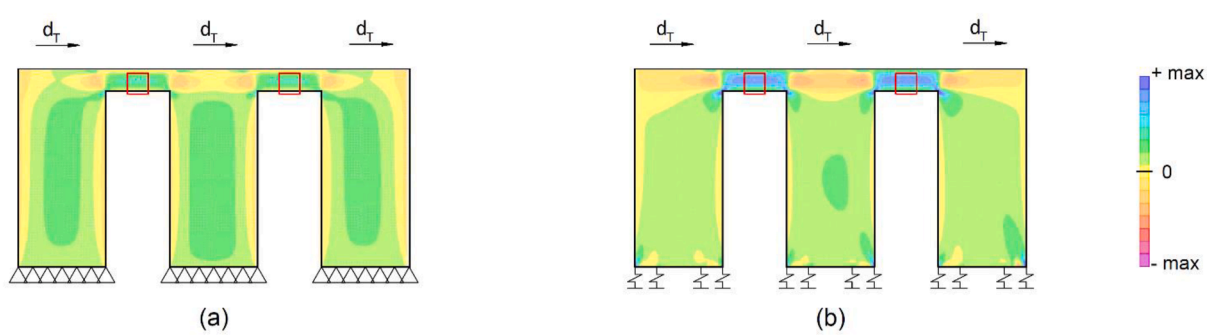

Fig. 7. Shear forces with (a) rigid and (b) flexible anchors - t = 100 mm, b = 1.20 m, hL = 0.30 m, l = 0.90 m.

maximum values are located in mid sections of wall segments (M-WS). In case of flexible anchors, the maximum values of shear forces are observed in the centre of mid sections of lintels (M-L) for lintel's length equal to 0.90 m, see Fig. 7, with the exception of the case with $b = 2.40$ m, $h_L = 0.75$ m, $l = 0.90$ m and hold-down stiffness $k_{h,z,t}$ equal to 13247 kN/m. When the lintel's length is equal to 2.10 m the maximum values are located in the top corners of door openings (C-DO), see Fig. 6b.

3.3. Location of the maximum values for shear-walls with window openings

The locations of maximum values of axial and shear forces per unit length are shown in Fig. 8 and reported in Table 5 for CLT walls with window openings of thickness equal to 100 mm and lintel's height and length equal to [0.30; 0.75]m and [0.90; 2.10]m, respectively. The maximum values of axial internal forces were identified at the Base-

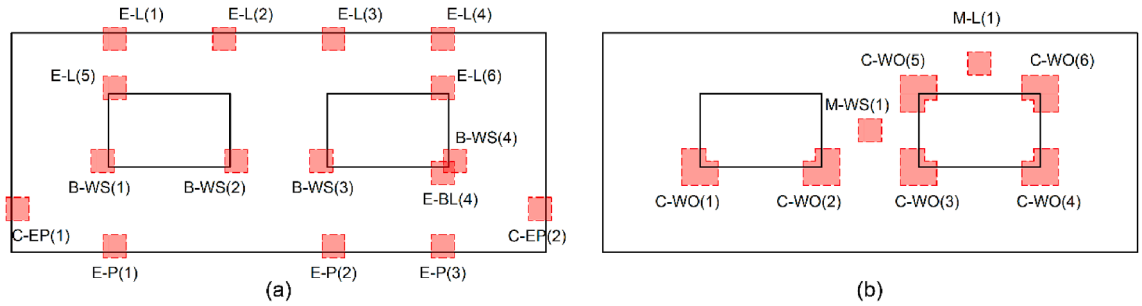

Fig. 8. Legend of locations for maximum values of internal (a) axial and (b) shear forces for shear-walls with window openings.

section of Wall Segments (B-WS), at the bottom Corners of the Entire Panel (C-EP), the End-section of Lintels (E-L) or Parapets (E-P). The maximum values of shear internal forces were detected on the contrary at the centre of the Mid-section of the inner Wall Segments (M-WS), at the centre of Mid-section of lintels (M-L) an at the corners around the window opening (C-WO).

The location of maximum values of axial forces in case of window opening is dependent on the aspect (length over height) ratio of lintels for the cases of flexible anchors while minor influence of the lintel aspect ratio is observed for the case with rigid anchors and wall segments widths equal to 1.80 m and 2.40 m. For slender lintels, namely length equal to 2.10 m and height equal to 0.30 m, the maximum values are located at the base of wall segments (B-WS), see Fig. 9a, and at the end sections of parapets (E-P), see Fig. 9b, for rigid and flexible anchors, respectively. For wide lintels, namely length equal to 0.90 m and height equal to 0.75 m, the maximum values are observed at the bottom corners of the entire panel in all cases (C-EP) both for rigid and flexible anchors, see Fig. 10a, with the exception of the case with a hold-down stiffness equal to 6609 kN/m and a wall segment width equal to 2.40 m. In case of lintels with height equal to 0.75 m and length equal to 2.10 m the maximum values of axial forces are detected at the end sections of lintels (E-L), see Fig. 10b, with exception of the case with rigid anchors and a width of the wall segment equal to 2.40 m.

The location of maximum values of shear forces is in all cases located in the corners around the window openings (C-WO), both for rigid and flexible anchors, see Fig. 11.

In Table 6, the cases of shear-walls with window openings with thickness equal to 160 mm which showed a different location from the cases with thickness equal to 100 mm are reported.

4. Distribution of shear and axial internal section forces per unit length

The distribution of the shear (v) and axial (n_x and n_z) internal forces per unit length was investigated in the relevant sections shown in Fig. 12, of the CLT shear-walls with flexible anchor systems where the maximum values of forces were detected by the analyses reported in the previous sections. The distribution of internal section forces has not been analysed in case of rigid anchors since this assumption cannot be considered realistic for most of hold-down and angle brackets commonly used nowadays to anchor CLT shear-walls to the foundation.

The distribution of internal axial and shear forces was obtained by plotting the values from the FE analyses with a spacing equal to 15 cm along each section. Analytical expressions for the internal forces per unit length are defined as function of the global actions on each section (i.e. axial load, shear load and bending moment) which were determined integrating the internal forces per unit length of the shell elements interested by the studied section. A comparison between the values of internal forces obtained from FE analyses and the analytical prediction is presented and discussed.

4.1. Door openings

4.1.1. Sections S_{D1} and S_{D3}

The distributions of the axial and shear forces per unit length obtained from the FE analyses in end sections of lintels S_{D1} and S_{D3}, see Fig. 13, are approximately linear for all analysed cases as shown in Fig. 14.

The analytical expression for the distribution of the axial forces $n_{x,SD1}(z)$ along the height of the section can be obtained from the "beam" theory [29] as function of the global axial force N_{SD1} and the bending moment M_{SD1}, as expressed by Eq. (7):

$$n_{x,SD1}(z) = \frac{N_{SD1}}{h_L} - \frac{12 \cdot M_{SD1}}{h_L^3} \cdot z \tag{7}$$

where z is the vertical distance from the centre of the section.

The analytical expression for the linear distribution of shear forces

Table 5
Location of maximum values of internal forces for walls with window openings - t = 100 mm.

t = 100 mm			Rigid [-]		Flexible $k_{h,z,t}$ = 6609 kN/m		$k_{h,z,t}$ = 13247 kN/m	
b [m]	h_L [m]	l [m]	Axial	Shear	Axial	Shear	Axial	Shear
1.20	0.30	2.10	B-WS $_{(2, 3)}$	C-WO $_{(1 \text{ to } 4)}$	E-P $_{(1, 3, 4)}$	C-WO $_{(3, 4)}$	E-P $_{(1, 3, 4)}$	C-WO $_{(3)}$
1.20	0.30	0.90	C-EP $_{(1, 2)}$ B-WS $_{(2, 3)}$	C-WO $_{(1 \text{ to } 4)}$	C-EP $_{(2)}$	C-WO $_{(4)}$	C-EP $_{(2)}$	C-WO $_{(4)}$
1.20	0.75	2.10	E-L $_{(1 \text{ to } 6)}$	C-WO $_{(1 \text{ to } 4)}$ M-WS $_{(1)}$	E-L $_{(3, 4, 6)}$	C-WO $_{(3, 4)}$	E-L $_{(3, 4, 6)}$	C-WO $_{(3, 4)}$
1.20	0.75	0.90	C-EP $_{(1, 2)}$	C-WO $_{(1 \text{ to } 4)}$ M-WS $_{(1)}$	C-EP $_{(2)}$	C-WO $_{(4)}$	C-EP $_{(2)}$	C-WO $_{(4 \text{ to } 6)}$ M-WS $_{(1)}$
1.80	0.30	2.10	B-WS $_{(2, 3)}$ C-EP $_{(1, 2)}$	C-WO $_{(1 \text{ to } 4)}$	E-P $_{(1, 4)}$	C-WO $_{(3, 4)}$	E-BL $_{(1, 4)}$	C-WO $_{(2 \text{ to } 4)}$
1.80	0.30	0.90	C-EP $_{(1, 2)}$	C-WO $_{(1 \text{ to } 4)}$	E-P $_{(1, 4)}$ E-L $_{(4)}$	C-WO $_{(3, 4)}$	C-EP $_{(2)}$	C-WO $_{(3, 4)}$
1.80	0.75	2.10	E-L $_{(1 \text{ to } 4)}$ C-EP $_{(1, 2)}$	C-WO $_{(1 \text{ to } 4)}$	E-L $_{(3, 4)}$	C-WO $_{(3, 4)}$	E-L $_{(3, 4)}$	C-WO $_{(3, 4)}$
1.80	0.75	0.90	C-EP $_{(1, 2)}$	C-WO $_{(1 \text{ to } 4)}$	C-EP $_{(2)}$	C-WO $_{(4)}$ M-WS $_{(1)}$	C-EP $_{(2)}$	C-WO $_{(4)}$ M-WS $_{(1)}$
2.40	0.30	2.10	B-WS $_{(1 \text{ to } 4)}$ C-EP $_{(1, 2)}$	C-WO $_{(1 \text{ to } 4)}$	E-P $_{(1)}$	C-WO $_{(3, 4)}$	E-P $_{(1)}$	C-WO $_{(2 \text{ to } 4)}$
2.40	0.30	0.90	C-EP $_{(1, 2)}$	C-WO $_{(1 \text{ to } 4)}$	E-P $_{(1, 2, 4)}$	C-WO $_{(3, 4)}$	C-EP $_{(2)}$	C-WO $_{(3, 4)}$
2.40	0.75	2.10	C-EP $_{(1, 2)}$	C-WO $_{(1 \text{ to } 4)}$	E-L $_{(3, 4)}$	C-WO $_{(3, 4)}$	E-L $_{(3, 4)}$	C-WO $_{(2 \text{ to } 4)}$
2.40	0.75	0.90	C-EP $_{(1, 2)}$	C-WO $_{(1 \text{ to } 4)}$ M-WS $_{(1)}$	E-L $_{(3, 4)}$	C-WO $_{(4)}$ M-WS $_{(1)}$	C-EP $_{(2)}$	C-WO $_{(4)}$ M-WS $_{(1)}$

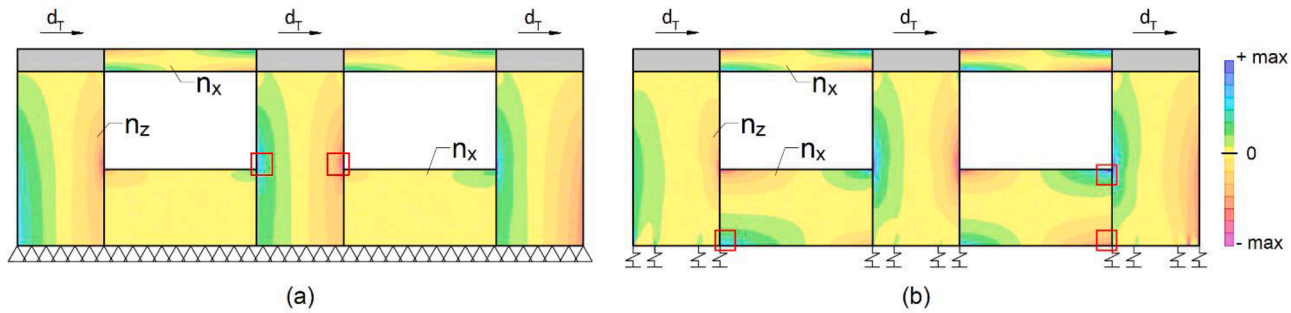

Fig. 9. Maximum values of axial forces in wall segments and lintels/parapets with (a) rigid and (b) flexible anchors - t = 100 mm, b = 1.20 m, h_L = 0.30 m, l = 2.10 m.

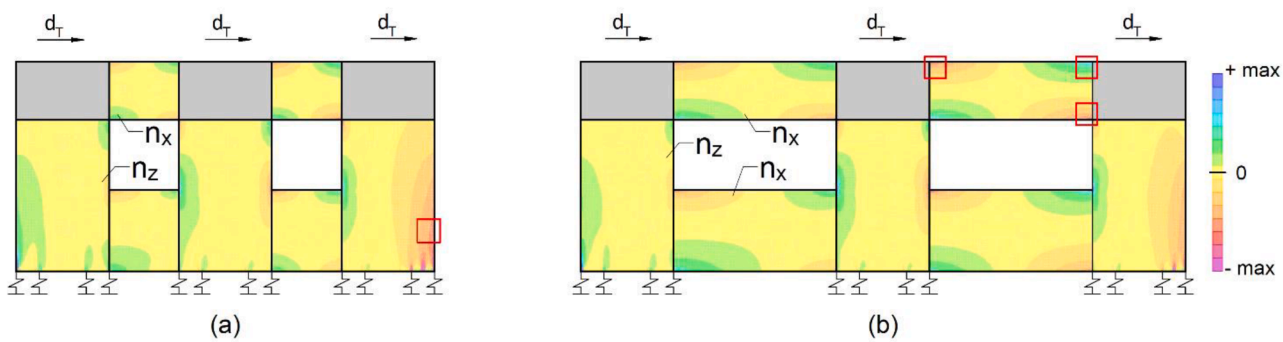

Fig. 10. Maximum values of axial internal forces in wall segments and lintels/parapets with flexible anchors - t = 100 mm, b = 1.20 m, h_L = 0.75 m, (a) l = 0.90 m and (b) l = 2.10 m.

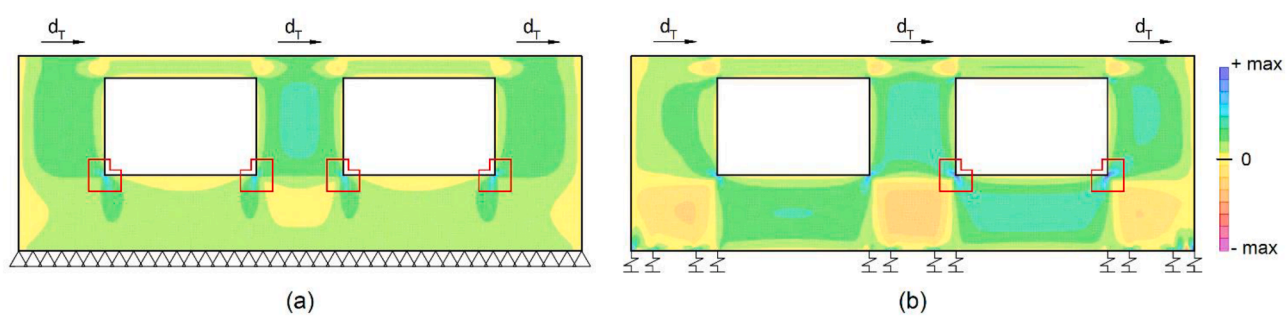

Fig. 11. Maximum values of shear forces with (a) rigid and (b) flexible anchors – t = 100 mm, b = 1.20 m, h_L = 2.10 m.

$v_{SD1}(z)$, see Eq. (8), is determined by assuming that the maximum value $v_{SD1,max}$ of shear forces is located next to the corner of the door opening, namely $z = -\frac{h_L}{2}$, and the integral of the shear internal forces along the height of the sections is equal to the global action V_{SD1}, as expressed by Eq. (9).

$$v_{SD1}(z) = \alpha \bullet z + \beta \tag{8}$$

$$\begin{cases} v_{SD1}\left(-\dfrac{h_L}{2}\right) = v_{SD1,max} \\ \displaystyle\int_{-h_L/2}^{h_L/2} v_{SD1}(z)dz = V_{SD1} \end{cases} \tag{9}$$

where α and β are the coefficients that are calculated by satisfying the two conditions of Eq. (9).

The FE analyses showed a linear dependency of the maximum value of shear forces $v_{SD1,max}$ on the ratio between the length of the lintel l and height of the door opening h_D. On the contrary a negligible dependency on the hold-down stiffness $k_{h,z,t}$ and length of wall segments b has been observed. As shown in Fig. 15, where $v_{u,SD1} = \frac{|V_{SD1}|}{h_L}$, for shear-walls with thickness equal to 100 mm, a good approximation of $v_{SD1,max}$ from the FE analyses can be expressed as:

$$v_{SD1,max} = \left(1.3 + 0.6 \bullet \frac{l}{h_D}\right) \bullet \frac{V_{SD1}}{h_L} \tag{10}$$

Eq. (8) can hence be rewritten as:

$$v_{SD1}(z) = \left[1 - \frac{z}{h_L} \bullet \left(0.6 + 1.2 \bullet \frac{l}{h_D}\right)\right] \bullet \frac{V_{SD1}}{h_L} \tag{11}$$

In Fig. 16, the distribution of axial and shear internal forces obtained from FE analyses and Eqs. (7) and (11), respectively, are reported for four different cases as normalized values to $n_{b,SD1} = \frac{6 \bullet |M_{SD1}|}{h_L^2}$ and $v_{u,SD1}$, showing that the influence of the geometric configuration on these particular sectional forces distribution is negligible.

Table 6
Locations of maximum values of internal forces for t = 160 mm for shear-wall with window openings.

t = 160 mm			Rigid		Flexible			
			[-]		$k_{h,z,t}$ = 6609 kN/m		$k_{h,z,t}$ = 13247 kN/m	
b [m]	h [m]	l [m]	Axial	Shear	Axial	Shear	Axial	Shear
1.20	0.30	2.10	B-WS $_{(2,\ 3)}$ C-EP $_{(1,\ 2)}$	C-WO $_{(1\ to\ 4)}$	–	–	–	–
1.20	0.75	2.10	C-EP $_{(1,\ 2)}$	C-WO $_{(1\ to\ 4)}$	–	–	–	–
1.80	0.30	0.90	–	–	C-EP $_{(1,\ 2)}$	C-WO $_{(3,\ 4)}$	–	–
2.40	0.30	0.90	–	–	C-EP $_{(1,\ 2)}$	C-WO $_{(3,\ 4)}$	–	–
2.40	0.75	0.90	–	–	C-EP $_{(1,\ 2)}$	C-WO $_{(4)}$ M-WS $_{(1)}$	–	–

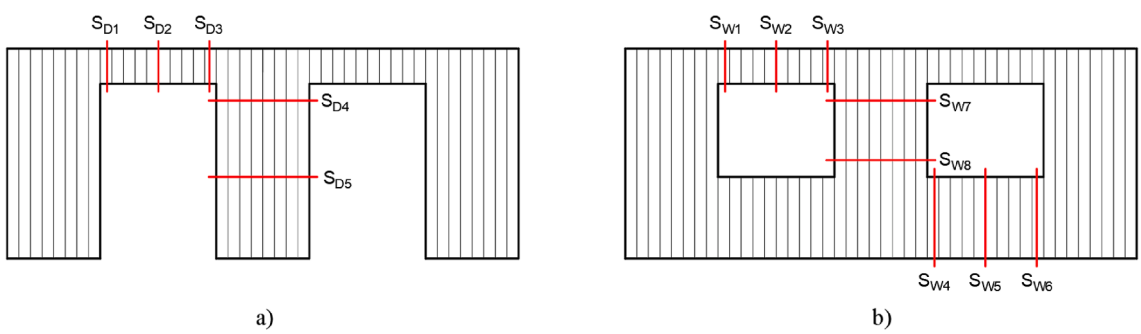

Fig. 12. Relevant sections of the CLT shear-walls with (a) door and (b) window openings.

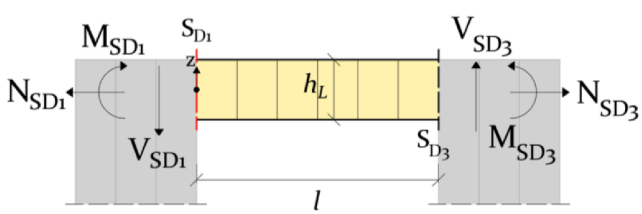

Fig. 13. Global actions on end sections of lintels S_{D1} and S_{D3}.

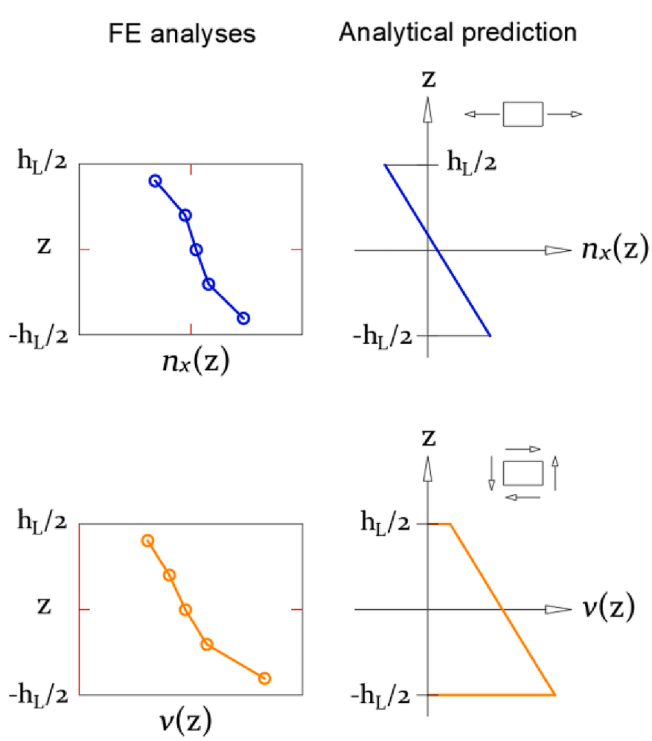

Fig. 14. Distribution of axial and shear forces for sections S_{D1} and S_{D3}.

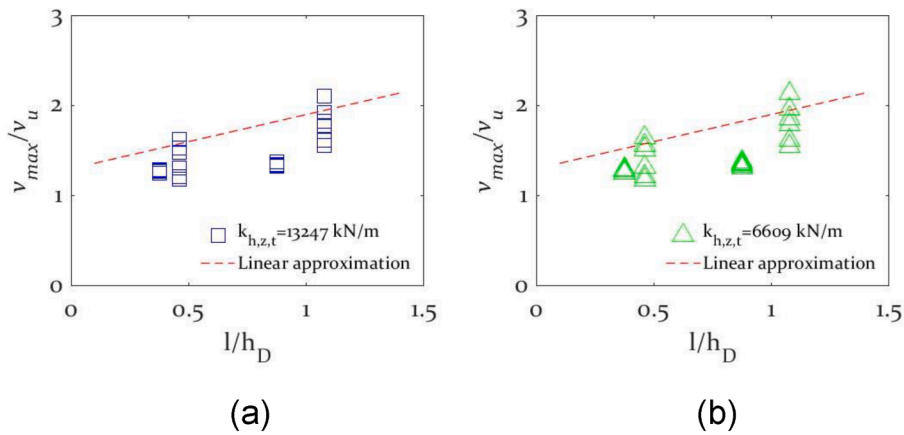

Fig. 15. *Normalized representation of* $v_{SD1,max}$ with $\mathbf{k}_{h,z,t}$ equal to (a) 13247 kN/m and (b) 6609 kN/m.

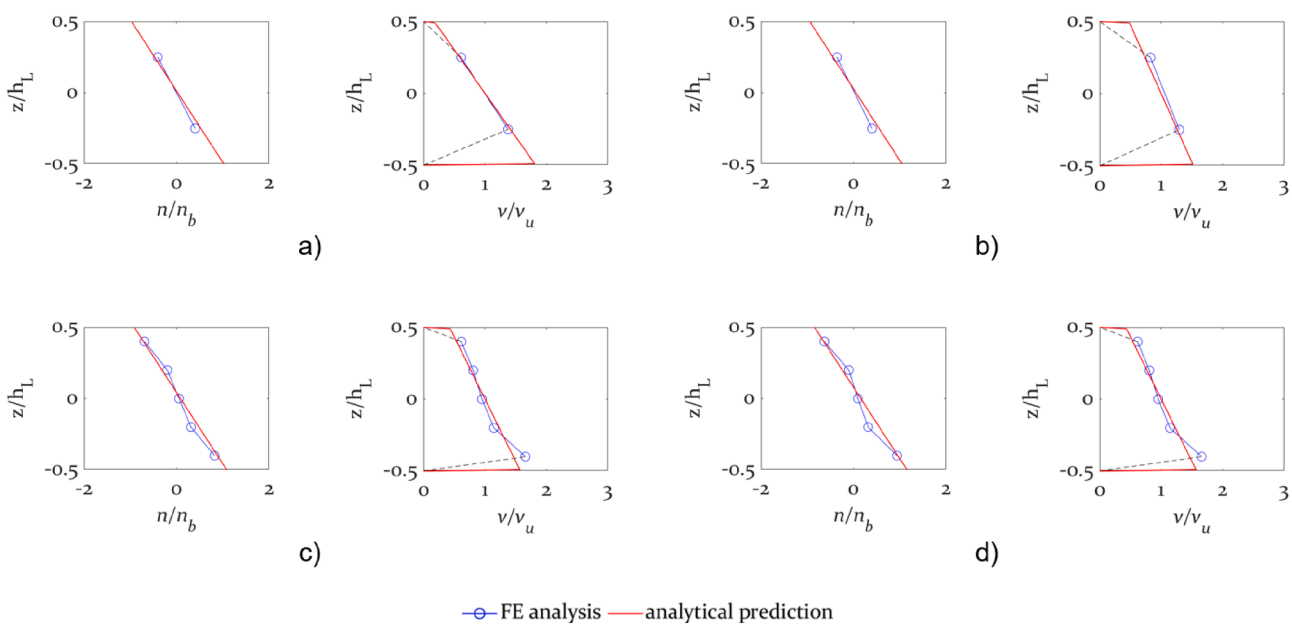

Fig. 16. Distribution of axial and shear internal forces per unit length along section S_{D1}; FE analyses (-o-) and analytical (-) prediction: a) l = 2.10 m, h_L = 0.30 m, b = 1.80 m; b) l = 0.90 m, h_L = 0.30 m, b = 1.80 m; c) l = 2.10 m, h_L = 0.75 m, b = 1.80 m; d) l = 0.90 m, h_L = 0.75 m, b = 1.80 m.

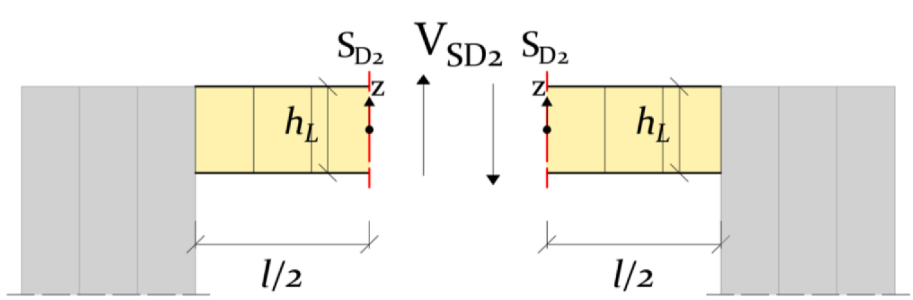

Fig. 17. Global actions on mid-section of lintel S_{D2}.

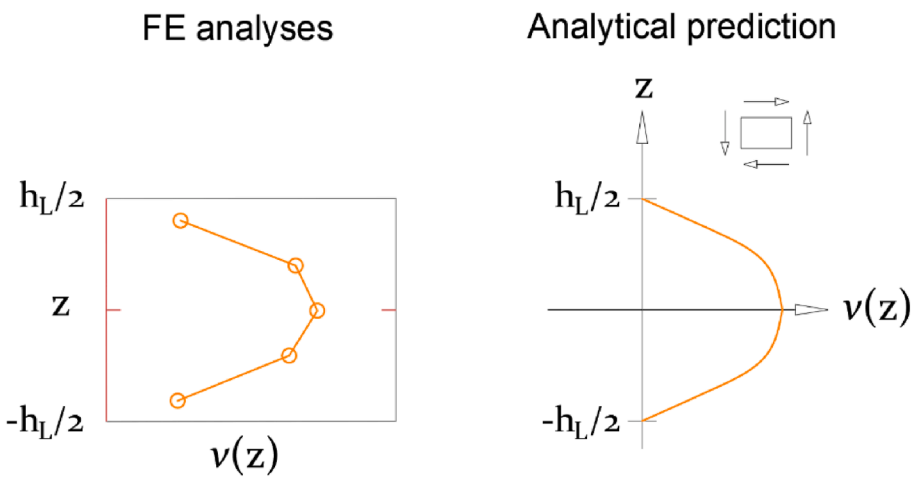

Fig. 18. Distribution of shear forces for section S_{D2}.

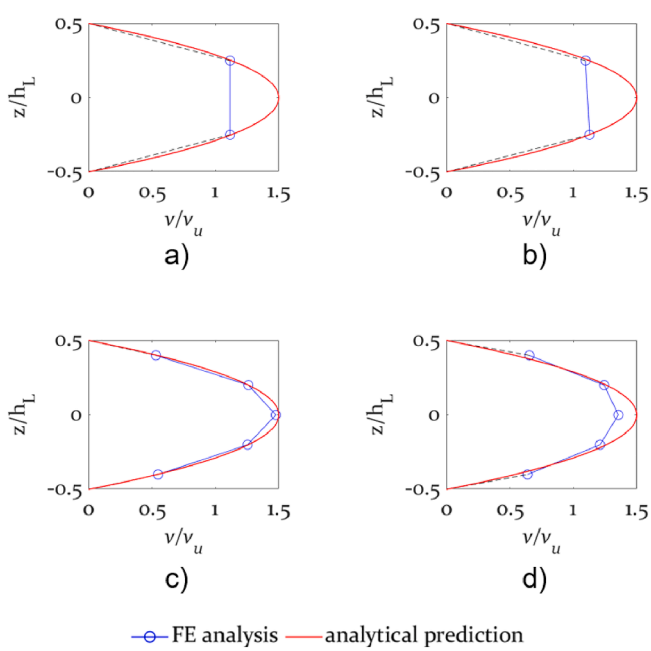

Fig. 19. Distribution of shear internal forces per unit length along section S_{D2}; FE analyses (-o-) and analytical (-): a) l = 2.10 m, h_L = 0.30 m, b = 1.80 m; b) l = 0.90 m, h_L = 0.30 m, b = 1.80 m c) l = 2.10 m, h_L = 0.75 m, b = 1.80 m; d) l = 0.90 m, h_L = 0.75 m, b = 1.80 m.

4.1.2. Section S_{D2}

In mid sections of lintels S_{D2} negligible values of axial forces are observed. The bending moment is in fact almost zero when shear-walls are subjected to horizontal forces. For this reason, only the distribution of internal shear forces is analysed for section S_{D2}, see Fig. 17.

The FE analyses showed that the distribution of shear forces $v_{SD2}(z)$ along section S_{D2} can be described by a quadratic function, Eq. (12), in accordance with the "Jourawski" theory [8] for beam elements with rectangular sections, as shown in Fig. 18.

The coefficients α, β and γ of Eq. (12) can be determined by assuming that: *i)* the maximum value is achieved in the centre of section, namely $z = 0$; *ii)* $v_{SD2,max}$ is equal to $\frac{3}{2}\bullet\frac{V_{SD2}}{h_L}$, *iii)* the integral of the internal shear forces is equal to the global action V_{SD2}.

$$v_{SD2}(z) = \alpha\bullet z^2 + \beta\bullet z + \gamma \tag{12}$$

$$\begin{cases} v_{SD2}'(0) = 0 \\ v_{SD2}(0) = v_{SD2,max} = \dfrac{3}{2}\bullet\dfrac{V_{SD2}}{h_L} \\ \displaystyle\int_{-h_L/2}^{h_L/2} v_{SD2}(z)dz = V_{SD2} \end{cases} \tag{13}$$

From Eqs. (9) and (10), we get:

$$v_{SD2}(z) = \left[\frac{3}{2} - 6\bullet\left(\frac{z}{h_L}\right)^2\right]\bullet\frac{V_{SD2}}{h_L} \tag{14}$$

In Fig. 19, the distributions of shear internal forces obtained from FE analyses and Eq. (14) are reported for four different cases as normalized values to $v_{u,SD2} = \frac{|V_{SD2}|}{h_L}$, showing that the influence of the geometric configuration on also these sectional forces distribution is negligible.

4.1.3. Section S_{D4}

The typical distributions of internal axial and shear forces obtained from the FE analyses on the section located on the top of wall segment S_{D4} is shown in Fig. 20. In Fig. 21 the global actions in terms of bending moment, shear and axial forces on section S_{D4} and on the two adjacent lintels are reported.

From the FE analyses it is observed that the distribution of axial forces per unit length $n_{z,SD4}(x)$ can be determined by the sum of three different contributions, see Eq. (15).

$$n_{z,SD4}(x) = n_{z,SD4,I}(x) + n_{z,SD4,II}(x) + n_{z,SD4,III}(x) \tag{15}$$

The first contribution, $n_{z,SD4,I}(x)$, takes into account the axial forces transmitted by the shear load $V_{L,l}$ of the adjacent lintel on the left. The FE analyses showed that the axial forces $n_{z,SD4,I}(x)$ are concentrated within a distance from the edge of the section $l_{L,nz,l}$ approximately equal to the height of the lintel $h_{L,l}$ and not greater than half of the wall segment

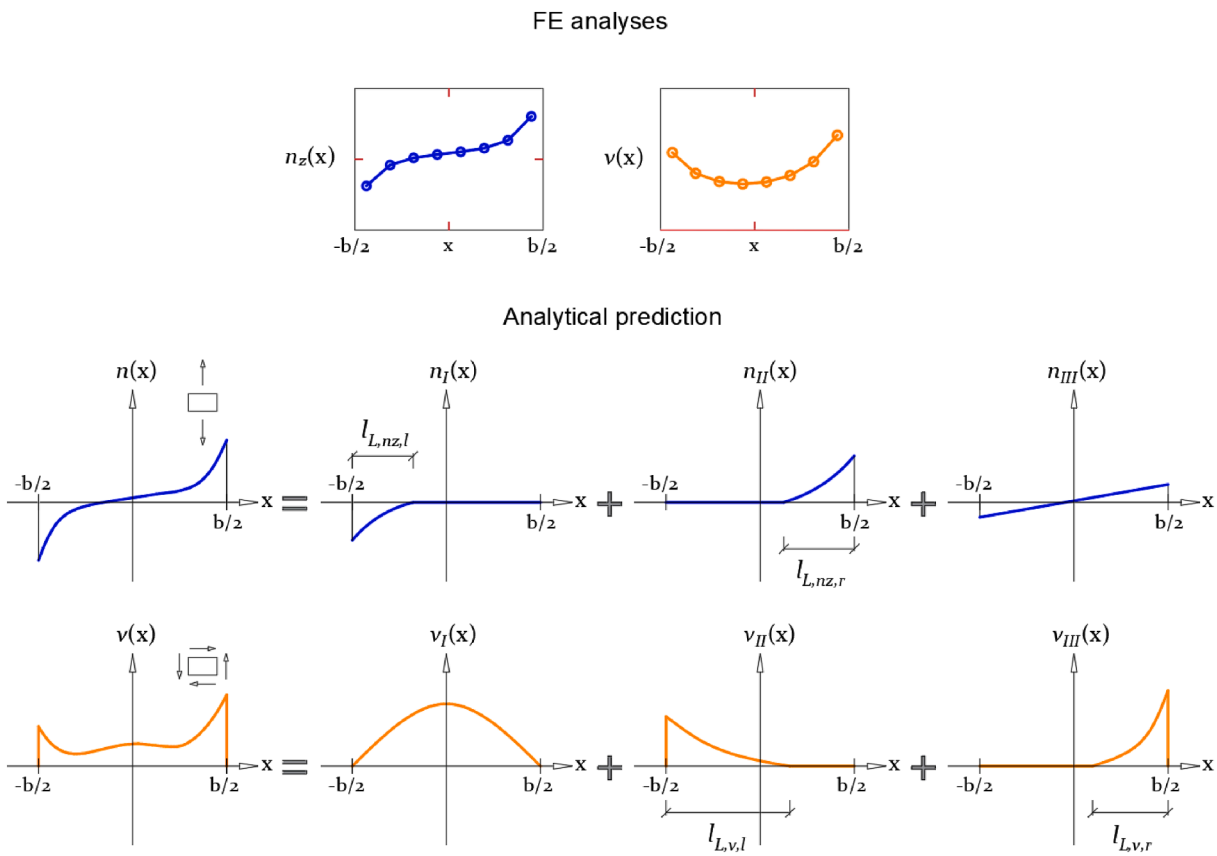

Fig. 20. Distribution of axial and shear forces for section S_{D4}.

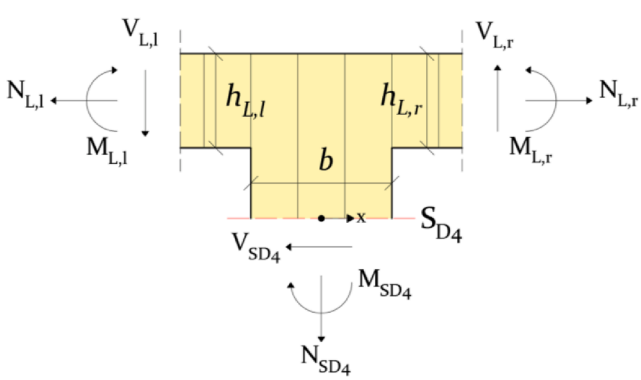

Fig. 21. Global actions on S_{D4} and the adjacent lintels.

width b, see Eq. (16).

$$l_{L,nz,l} = \begin{cases} h_{L,l} & for\ \ h_{L,l} \le \dfrac{b}{2} \\ \dfrac{b}{2} & for\ \ h_{L,l} > \dfrac{b}{2} \end{cases} \tag{16}$$

A quadratic expression can be adopted for the analytical prediction of $n_{z,SD4,I}(x)$ as reported in Eq. (17).

$$n_{z,SD4,I}(x) = \begin{cases} \alpha \bullet z^2 + \beta \bullet z + \gamma & \text{for} \quad x \le -\dfrac{b}{2} + l_{L,nz,l} \\ 0 \quad \text{for} \quad x > -\dfrac{b}{2} + l_{L,nz,l} \end{cases} \tag{17}$$

where x is the horizontal distance from the centre of the section.

The coefficients α, β and γ are determined by three conditions: *i)* the quadratic function is equal to zero for $x = -\frac{b}{2} + l_{L,nz,l}$ in order to ensure the continuity of function $n_{z,SD4,I}(x)$ along the entire section; *ii)* the maximum value $n_{z,SD4,I,max}$ is achieved on the edge of the section adjacent to the lintel; *iii)* the integral of $n_{z,SD4,I}(x)$ is equal to the shear load of the adjacent lintel $V_{L,l}$.

$$\begin{cases} n_{z,SD4,I}\left(-\dfrac{b}{2} + l_{L,nz,l}\right) = 0 \\ n_{z,SD4,I}\left(-\dfrac{b}{2}\right) = n_{z,SD4,I,max} \\ \displaystyle\int_{-b/2}^{b/2} n_{z,SD4,I}(x)dx = V_{L,l} \end{cases} \tag{18}$$

The FE analyses showed that the maximum value $n_{z,SD4,I,max}$ can be expressed as:

$$n_{z,SD4,I,max} = -\frac{3 \bullet V_{L,l}}{l_{L,nz,l}} \tag{19}$$

From Eqs. (17)–(19), Eq. (17) can hence be rewritten as:

$$n_{z,SD4,I}(x) = \begin{cases} -\dfrac{3 \bullet V_{L,l}}{l_{L,nz,l}^{\ 3}} \bullet \left[x + \dfrac{b}{2} - l_{L,nz,l}\right]^2 & for \quad x \le -\dfrac{b}{2} + l_{L,nz,l} \\ 0 \quad for \quad x > -\dfrac{b}{2} + l_{L,nz,l} \end{cases} \tag{20}$$

The second contribution $n_{z,SD4,II}(x)$ is similar to $n_{z,SD4,I}(x)$ since related

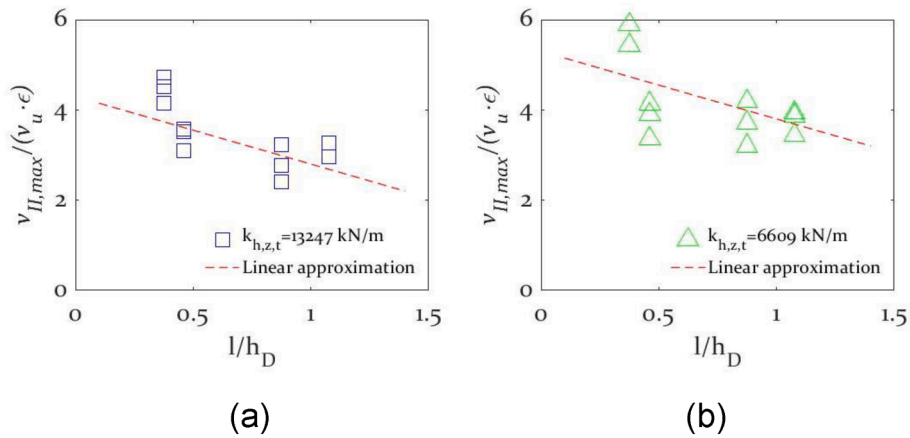

Fig. 22. Normalized representation of $v_{SD4,II,max}$ with $k_{h,z,t}$ equal to (a) 13247 kN/m and (b) 6609 kN/m.

to the shear action $V_{L,r}$ transmitted by the adjacent lintel on the right. The analytical expression for $n_{z,SD4,II}(x)$ can hence be expressed as:

$$n_{z,SD4,II}(x) = \begin{cases} 0 \quad for \quad x < \frac{b}{2} - l_{L,nz,r} \\ \frac{3 \bullet V_{L,r}}{l_{L,nz,r}^{3}} \bullet \left[x - \frac{b}{2} + l_{L,nz,r}\right]^2 \quad for \quad x \geq \frac{b}{2} - l_{L,nz,r} \end{cases} \tag{21}$$

where

$$l_{L,nz,r} = \begin{cases} h_{L,r} \quad for \quad h_{L,r} \leq \frac{b}{2} \\ \frac{b}{2} \quad for \quad h_{L,r} > \frac{b}{2} \end{cases} \tag{22}$$

The third contribution $n_{z,SD4,III}(x)$ can be expressed by a linear distribution as assumed for the "beam" theory [29]. In order that the internal translational and rotational equilibrium of the section is satisfied, namely $\int_{-b/2}^{b/2} n_{z,SD4}(x)dx = N_{SD4}$ and $\int_{-b/2}^{b/2} n_{z,SD4}(x)xdx = M_{SD4}$, the contributions due to the shear load of adjacent lintels $V_{L,l}$ and $V_{L,r}$ need to be taken into account in Eq. (23).

$$n_{z,SD4,III}(x) = \frac{N_{SD4} + V_{L,l} - V_{L,r}}{b} + \frac{12 \bullet \left[M_{SD4} - \left(V_{L,l} + V_{L,r}\right) \bullet \frac{b}{2}\right]}{b^3} \bullet x \tag{23}$$

As for the axial forces, the distribution of shear forces $v_{SD4}(x)$ can be obtained as the sum of three different contributions (Eq. (24)) which are described by three distribution functions $v_i(x)$ and three weighting coefficient $0 \leq w_i \leq 1$ ($\sum w_i = 1$), with i from I to III.

$$v_{SD4}(x) = v_{SD4,I}(x) \bullet w_I + v_{SD4,II}(x) \bullet w_{II} + v_{SD4,III}(x) \bullet w_{III} \tag{24}$$

In order to ensure the integral of shear force on the length of section $SD4$ is equal to the global shear action on the section, namely $\int_{-b/2}^{b/2} v_{SD4}(x)dx = V_{SD4}$, Eq. (25) is to be satisfied:

$$\int_{-b/2}^{b/2} v_{SD4,j}(x)dx = V_{SD4} \quad for \quad j = I, II, III \tag{25}$$

The distribution function related to the first contribution, $v_{SD4,I}(x)$, can be described by the "Jourawski" theory for beam elements with rectangular sections. By applying the same procedure presented for section S_{D2}, the analytical expression for the distribution function $v_{SD4,I}(x)$ can be written as:

$$v_{SD4,I}(x) = \left[\frac{3}{2} - 6 \bullet \left(\frac{x}{b}\right)^2\right] \bullet \frac{V_{SD4}}{b} \tag{26}$$

A quadratic expression, Eq. (27), can be used for the distribution function the second contribution $v_{SD4,II}(x)$. FE analyses showed that the shear forces $v_{SD4,II}(x)$ are related to the shear action $V_{L,l}$ transmitted by the adjacent lintel on the left and are concentrated within a distance $l_{L,v,l}$ from the edge of the section. It is also observed that the maximum value $v_{SD4,II,max}$ is achieved next to the corner of the left door opening, namely $x = -\frac{b}{2}$.

$$v_{SD4,II}(x) = \begin{cases} \alpha \bullet x^2 + \beta \bullet x + \gamma \quad for \quad x \leq -\frac{b}{2} + l_{L,v,l} \\ 0 \quad for \quad x > -\frac{b}{2} + l_{L,v,l} \end{cases} \tag{27}$$

where the coefficients α, β and γ are determined the conditions reported in Eq. (28).

$$\begin{cases} v_{SD4,II}\left(-\frac{b}{2} + l_{L,v,l}\right) = 0 \\ v_{SD4,II}\left(-\frac{b}{2}\right) = v_{SD4,II,max} \\ \int_{-b/2}^{b/2} v_{SD4,II}(x)dx = V_{SD4} \end{cases} \tag{28}$$

The FE analyses showed that the length $l_{L,v,l}$ is decreasing with the maximum value $v_{SD4,II,max}$ as expressed in Eq. (29).

$$l_{L,v,l} = \frac{3}{v_{SD4,II,max}} \bullet V_{SD4} \tag{29}$$

The maximum value $v_{SD4,II,max}$ of the distribution function is dependent on the ratio between the lintel length l and the height of the door opening h_D as well as on the tensile stiffness of the hold-down $k_{h,z,t}$, as reported in Eq. (30) and shown in Fig. 22, where $v_{u,SD4} = \frac{|V_{SD4}|}{b}$.

$$v_{SD4,II,max} = \left[5.3 \bullet \left(\frac{6609}{k_{h,z,t}}\right)^{0.3} - 1.5 \bullet \frac{1}{h_D}\right] \bullet \varepsilon_{v,SD4,II} \bullet \frac{V_{SD4}}{b} \tag{30}$$

where $k_{h,z,t}$ is expressed in [kN/m] and the coefficient $\varepsilon_{v,SD4,II}$ takes into account the contributions of the shear action on the wall segment V_{SD4} and the shear action transmitted by the adjacent lintel $V_{L,l}$, respectively, see Eq. (31).

$$\varepsilon_{v,SD4,II} = \left[1 + \frac{|V_{SD4}|}{|V_{L,l}|} \bullet \frac{h_{L,l}}{b}\right] \tag{31}$$

The Eq. (27) can hence be rewritten as

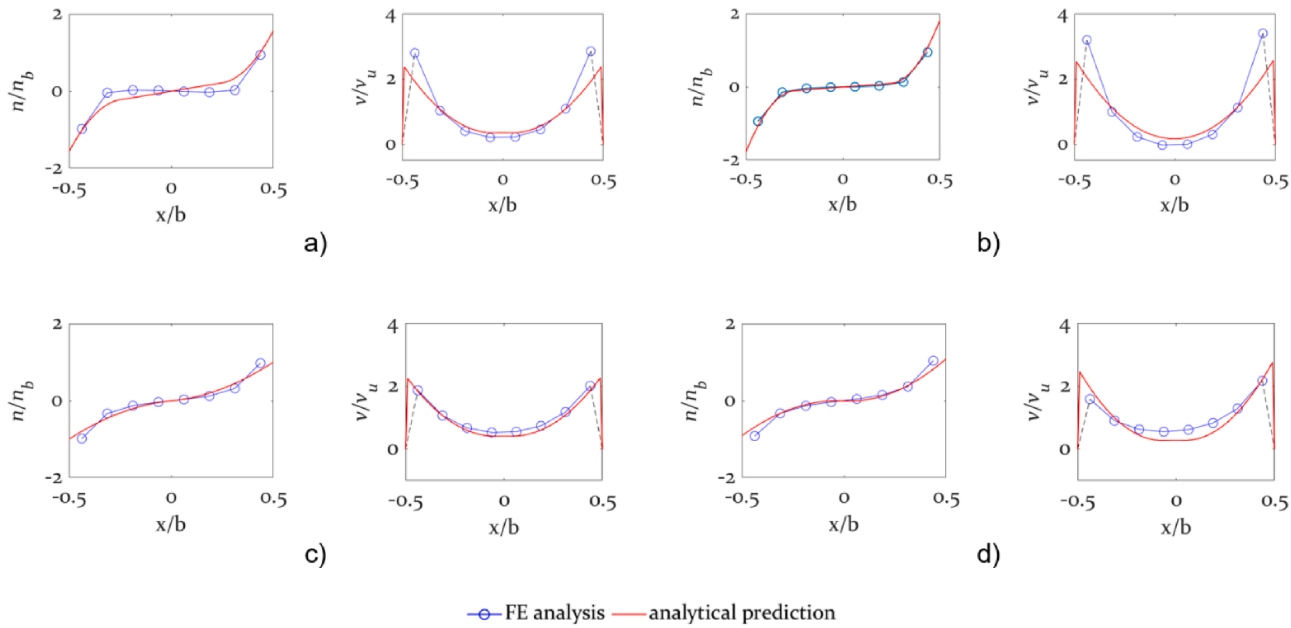

Fig. 23. Distribution of axial and shear forces per unit length along section S_{D4}; FE analyses (-o-) and analytical (-) prediction: a) l = 2.10 m, h_L = 0.30 m, b = 1.80 m; b) l = 0.90 m, h_L = 0.30 m, b = 1.80 m; c) l = 2.10 m, h_L = 0.75 m, b = 1.80 m; d) l = 0.90 m, h_L = 0.75 m, b = 1.80 m.

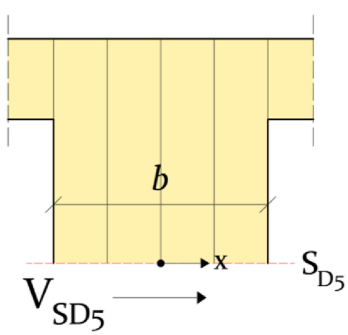

Fig. 24. Global actions on mid-section of wall segments S_{D5}.

$$v_{SD4,II}(x) = \begin{cases} \frac{1}{9}\bullet\left(\frac{v_{SD4,II,max}}{V_{SD4}}\right)^3\bullet\left[x+\frac{b}{2}-l_{L,v,l}\right]^2\bullet V_{SD4} & \text{for} \quad x \\ \leq -\frac{b}{2}+l_{L,v,l}0 & \text{for} \quad x > -\frac{b}{2}+l_{L,v,l} \end{cases} \tag{32}$$

The distribution function related to the third contribution $v_{SD4,III}(x)$ is specular to the function used for the second contribution $v_{SD4,II}(x)$ and related to the shear load transmitted by the adjacent lintel $V_{L,r}$, as reported in Eq. (33):

$$v_{SD4,III}(x) = \begin{cases} 0 \quad for \quad x \leq \frac{b}{2}-l_{L,v,r} \\ \frac{1}{9}\bullet\left(\frac{v_{SD4,II,max}}{V_{SD4}}\right)^3\bullet\left[x-\frac{b}{2}+l_{L,v,r}\right]^2\bullet V_{SD4} \quad for \quad x > -\frac{b}{2}+l_{L,v,r} \end{cases} \tag{33}$$

where

$$v_{SD4,III,max} = \left[5.3\bullet\left(\frac{6609}{k_{h,z,t}}\right)^{0.3} - 1.5\bullet\frac{l}{h_D}\right]\bullet\varepsilon_{v,SD4,III}\bullet\frac{V_{SD4}}{b} \tag{34}$$

$$\varepsilon_{v,SD4,III} = \left[1+\frac{|V_{SD4}|}{|V_{L,r}|}\bullet\frac{h_{L,r}}{b}\right] \tag{35}$$

$$l_{L,v,r} = \frac{3}{v_{SD4,III,max}}\bullet V_{SD4} \tag{36}$$

The weighting function $w_{i=I,II,III}$ which are used to take into account the three different contributions of the shear actions on the wall segments V_{SD4} and on the adjacent lintels $V_{L,l}, V_{L,r}$ can be expressed as:

$$w_I = \frac{|V_{SD4}/b|}{|V_{SD4}/b|+|V_{L,l}/h_{L,l}|+|V_{L,r}/h_{L,r}|} \tag{37}$$

$$w_{II} = \frac{|V_{L,l}/h_{L,l}|}{|V_{SD4}/b|+|V_{L,l}/h_{L,l}|+|V_{L,r}/h_{L,r}|} \tag{38}$$

$$w_{III} = \frac{|V_{L,r}/h_{L,r}|}{|V_{SD4}/b|+|V_{L,l}/h_{L,l}|+|V_{L,r}/h_{L,r}|} \tag{39}$$

In Fig. 23, the comparison between the values of axial as well as shear internal forces obtained from FE analyses and analytical prediction is shown for four different cases, as normalized values to $n_{b,SD4} = \frac{6\bullet|M_{SD4}|}{b^2}$ and $v_{u,SD4} = \frac{|V_{SD4}|}{b}$.

4.1.4. Section S_{D5}

Similarly to the midsection of lintels, negligible values of axial forces

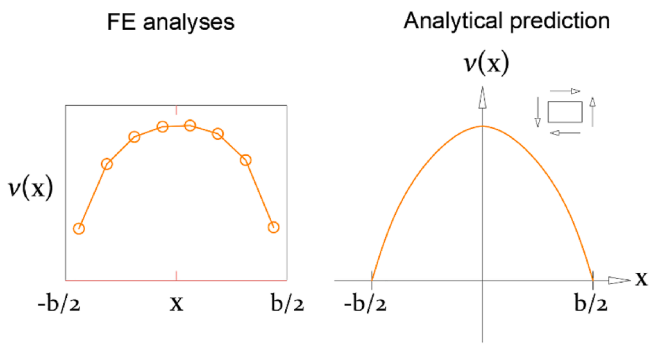

Fig. 25. Distribution of axial and shear forces for section S_{D5}.

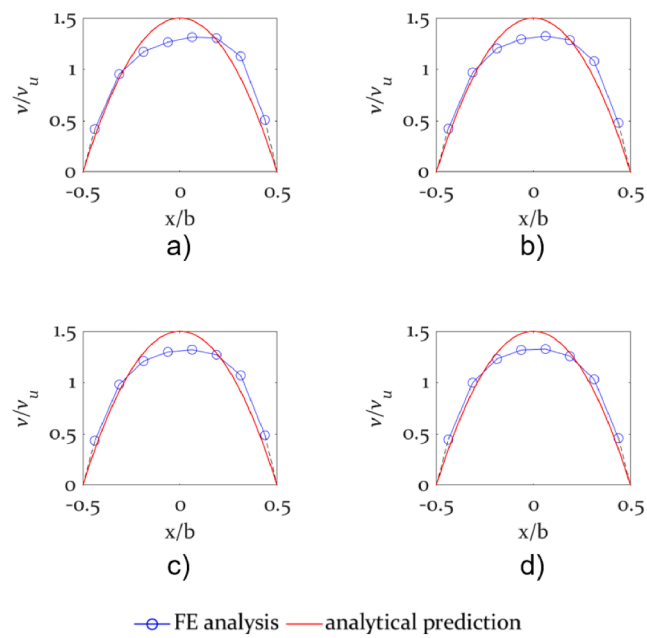

Fig. 26. Distribution of shear forces per unit length along section S_{D5}; FE analyses (-o-) and analytical (-): a) l = 2.10 m, h_L = 0.30 m, b = 1.80 m; b) l = 0.90 m, h_L = 0.30 m, b = 1.80 m; c) l = 2.10 m, h_L = 0.75 m, b = 1.80 m; d) l = 0.90 m, h_L = 0.75 m, b = 1.80 *m*.

are observed in the midsection S_{D5} of wall segments. For this reason, only the distributions of shear forces are analysed for this section.

From FE analyses, the distribution of shear force per unit length $v_{SD5}(x)$ can be described by the quadratic function, Eq. (40), in accordance with the "Jourawski" theory for beam elements with rectangular sections [8], see Figs. 24 and 25, getting:

$$v_{SD5}(x) = \left[\frac{3}{2} - 6\bullet\left(\frac{x}{b}\right)^2\right]\bullet\frac{V_{SD5}}{b} \tag{40}$$

In Fig. 26, the comparison between the values of shear internal forces obtained from FE analyses and given by Eq. (40) is reported for four different cases, as normalized values to $v_{u,SD5} = \frac{|V_{SD5}|}{b}$, showing that the influence of the geometric configuration on these particular forces distribution is negligible.

4.2. Window openings

4.2.1. Section S_{W1} and S_{W3}

The distribution of the axial and shear forces per unit length observed from the FE analyses on the end sections in lintels in the shear-walls with window openings S_{W1} and S_{W3}, are the same of those determined for shear-walls with door openings. Eq. (7) can be adopted for the analytical prediction of axial forces $n_{x,SW1}(z)$ and the same procedure adopted for section S_{D1} can be used to determine the analytical expression of the internal shear forces on sections S_{W1} and S_{W3}. The maximum values of the internal shear forces are expressed by Eq. (41) and shown in Fig. 27 where $v_{u,SW1} = \frac{|V_{SW1}|}{h_L}$.

$$v_{SW1,max} = \left(1.1 + 0.2\bullet\frac{l}{h_W}\right)\bullet\frac{V_{SW1}}{h_L} \tag{41}$$

The expression for the distribution of the internal shear forces can hence be expressed as:

$$v_{SW1}(z) = \left[1 - \frac{z}{h_L}\bullet\left(0.2 + 0.4\bullet\frac{l}{h_W}\right)\right]\bullet\frac{V_{SW1}}{h_L} \tag{42}$$

4.2.2. Section S_{W2} and S_{W5}

The distribution of internal shear forces mid sections of lintels and parapets in CLT shear-walls with window opening is the same of the distribution observed for mid sections of lintels in the cases with door openings. Eq. (14) can hence be adopted.

4.2.3. Section S_{W4} and S_{W6}

As for the lintels, a linear distribution of internal axial and shear forces was observed from the FE analyses along the end sections of

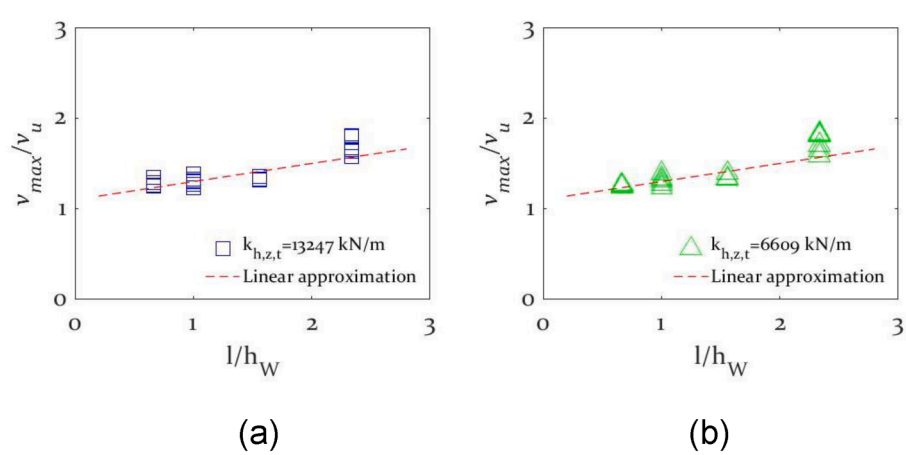

Fig. 27. Normalized representation of $\mathbf{v_{SW1,max}}$ with $\mathbf{k_{h,z,t}}$equal to (a) 13247 kN/m and (b) 6609 kN/m.

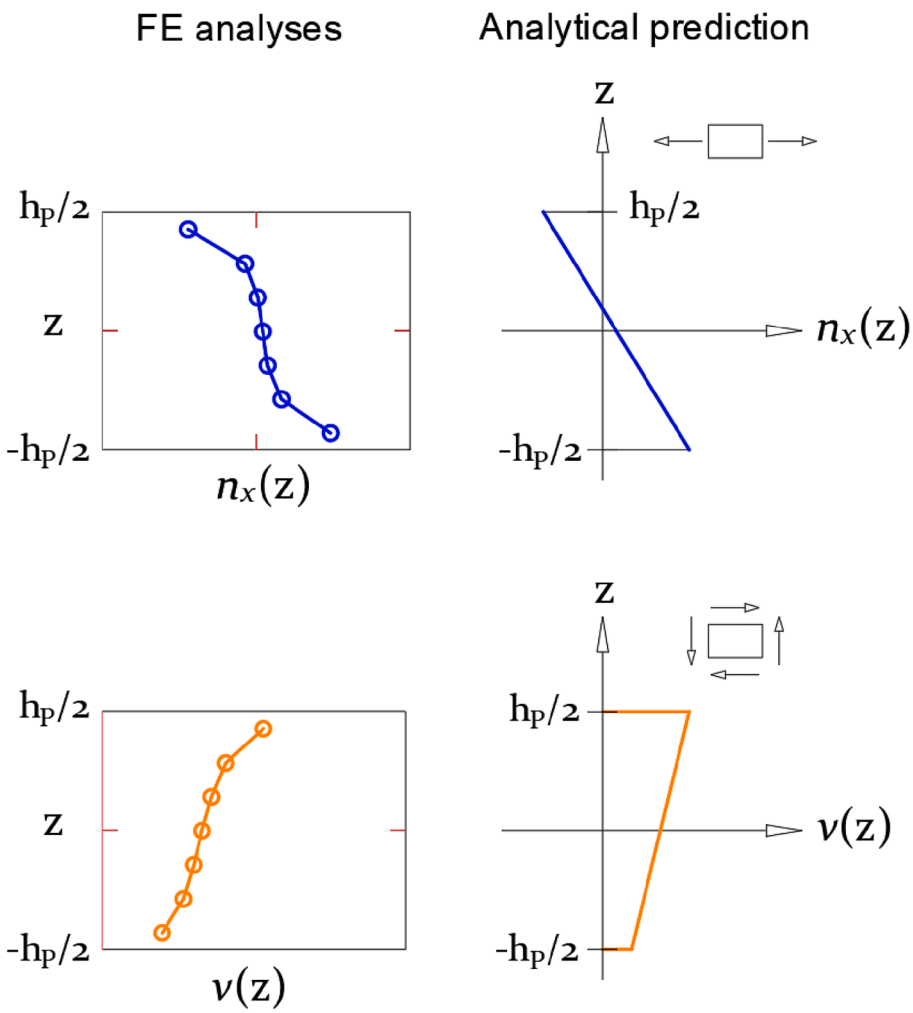

Fig. 28. Distribution of axial and shear forces for section S_{W4}.

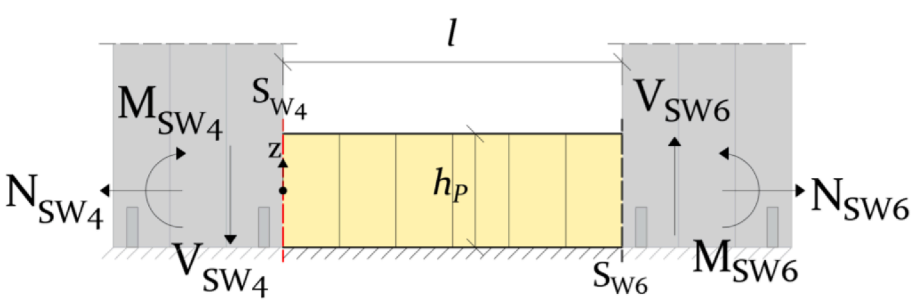

Fig. 29. Global actions on mid-section of wall segments SW4 and SW6.

parapets S_{W4}, as shown in Fig. 28. Eq. (7) can be adopted for the analytical prediction of axial forces $n_{x,SW4}(z)$ from the global axial force N_{SW4} and bending moment M_{SW4} (see Fig. 29).

The same procedure described for end section of lintels in door opening can be adopted to determine the analytical expressions for the distribution of internal shear forces $v_{SW4}(z)$ in the parapets. The FE analyses showed that the maximum value of shear forces $v_{SW4,max}$ is located next to the corner of the window opening and can be expressed as reported in Eq. (43) according to the linear approximation shown in Fig. 30.

$$v_{SW4,max} = \left(1.3 + 0.6 \bullet \frac{1}{h_W}\right) \bullet \frac{V_{SW4}}{h_P} \tag{43}$$

In Fig. 31, the comparison between the values of shear forces obtained from FE analyses and Eq. (44) is shown for four different cases, as normalized values to $v_{u,SW4} = \frac{|V_{SW4}|}{h_L}$.

$$v_{SW4}(z) = \left[1 + \frac{z}{h_P} \bullet \left(0.6 + 1.2 \bullet \frac{1}{h_W}\right)\right] \bullet \frac{V_{SW4}}{h_P} \tag{44}$$

The axial and shear forces per unit length distributions from FE and analytical models are shown in Fig. 31, where four different geometric configurations are taken into account, as normalized values to $n_{b,SW4} = \frac{6 \bullet |M_{SW4}|}{{h_P}^2}$ and $v_{u,SW4}$.

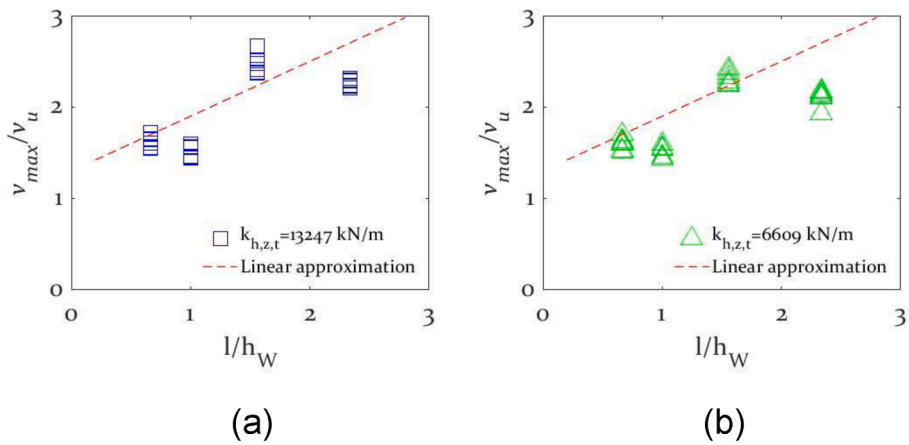

Fig. 30. Normalized representation of $\mathbf{v_{SW14,max}}$ with $\mathbf{k_{h,z,t}}$equal to (a) 13247 kN/m and (b) 6609 kN/m.

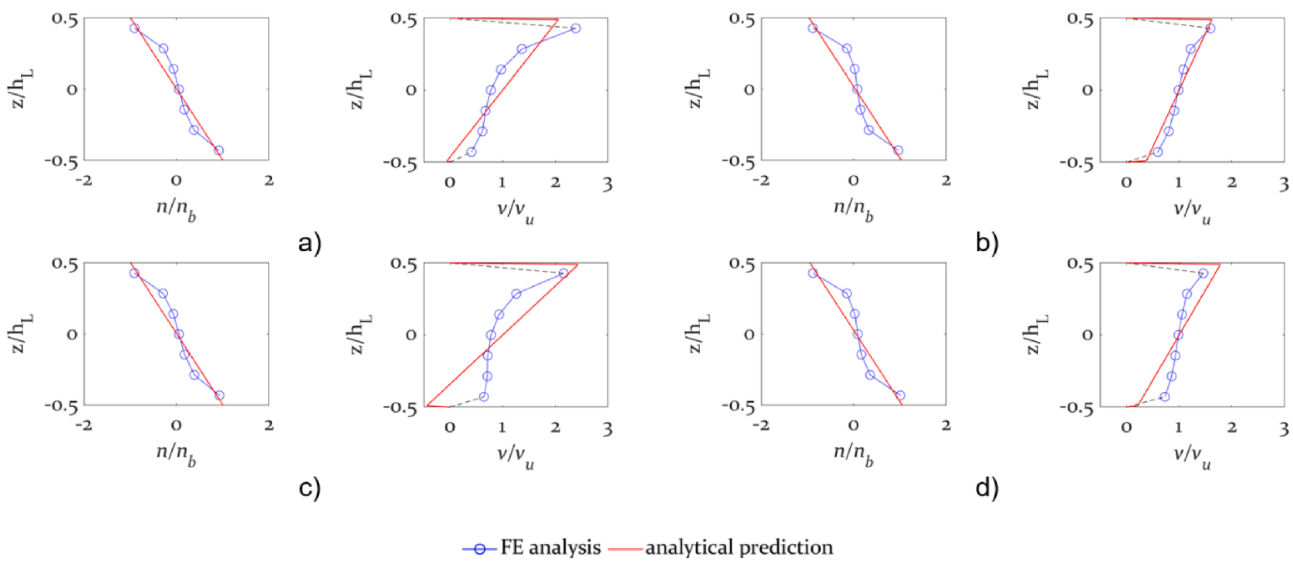

Fig. 31. Distribution of axial and shear internal forces per unit length along section S_{W4}; FE analyses (-o-) and analytical (-): a) l = 2.10 m, h_L = 0.30 m, b = 1.80 m; b) l = 0.90 m, h_L = 0.30 m, b = 1.80 m; c) l = 2.10 m, h_L = 0.75 m, b = 1.80 m; d) l = 0.90 m, h_L = 0.75 m, b = 1.80 *m.*

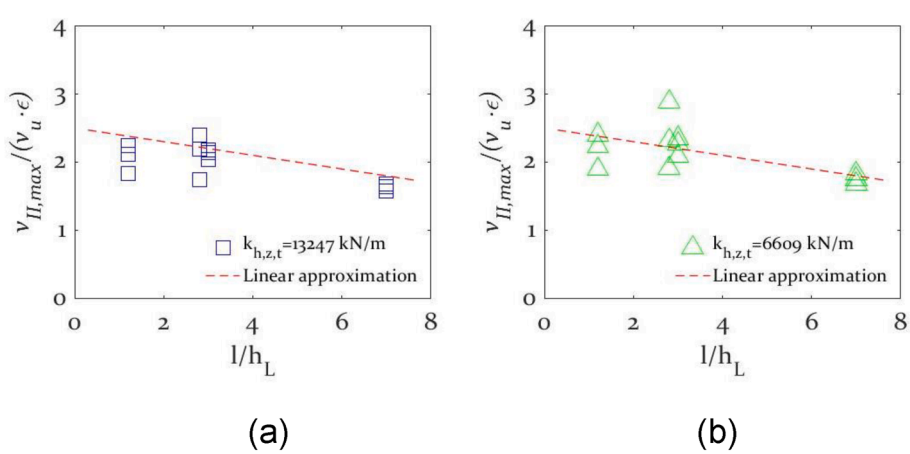

Fig. 32. Normalized representation of $\mathbf{v_{SW4,max}}$ with $\mathbf{k_{h,z,t}}$equal to (a) 13247 kN/m and (b) 6609 kN/m.

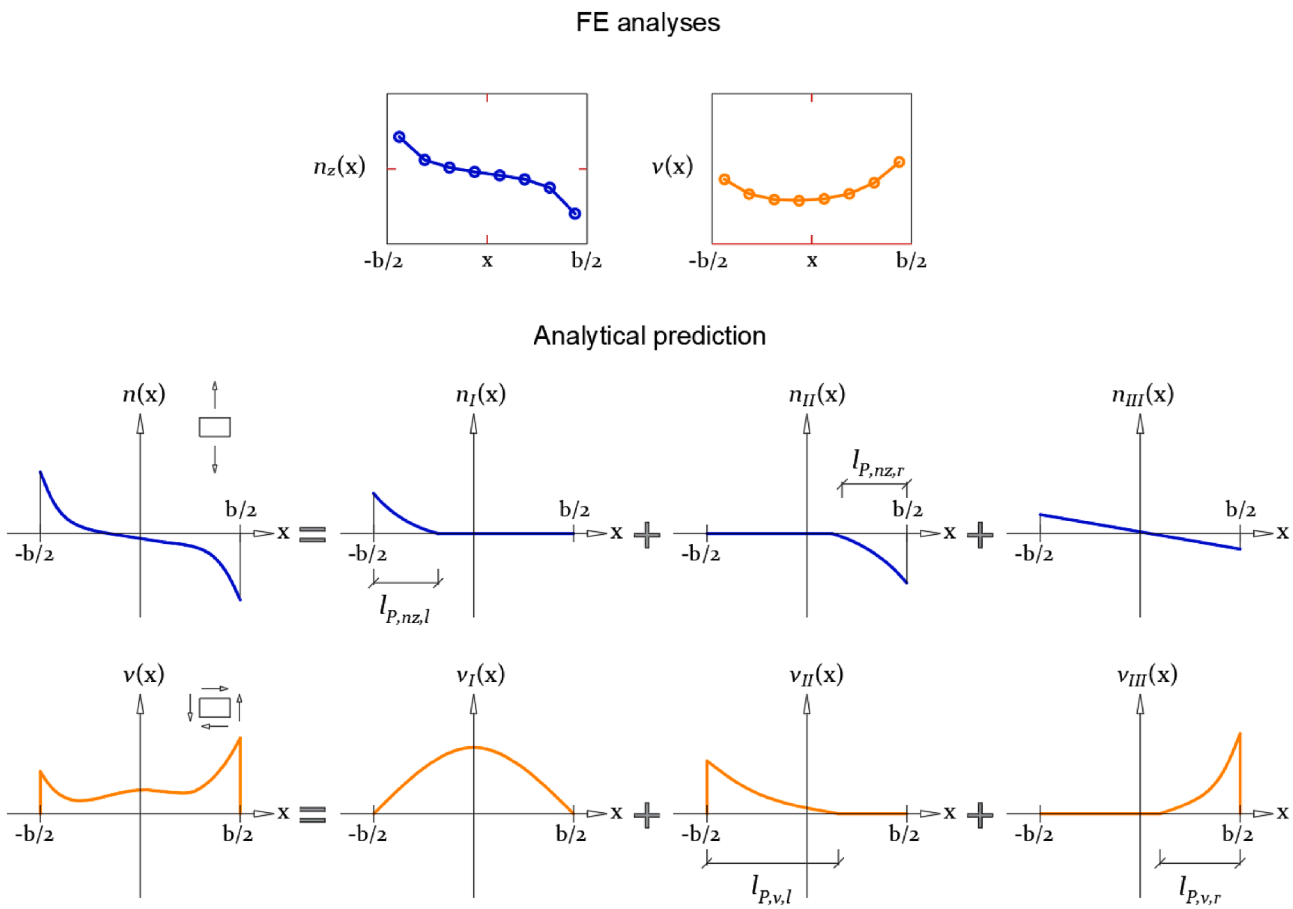

Fig. 33. Distribution of axial and shear forces for section S_{W8}.

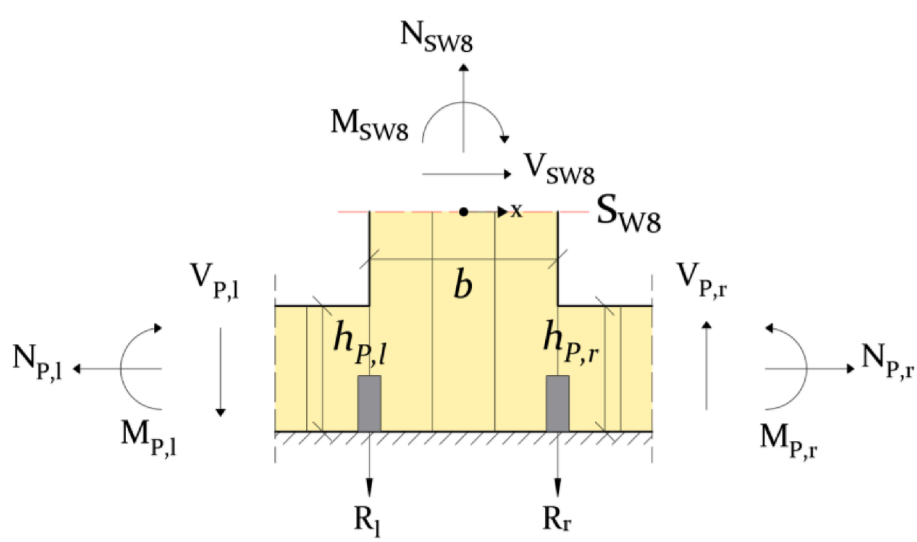

Fig. 34. Global actions on bottom section of wall segment S_{W8} and on adjacent parapets.

4.2.4. Section S_{W7}

The distributions of axial and shear forces observed in the top section of wall segments in case of window openings are similar to those observed in case of door openings. Eqs. (15)–(23) are still valid for the prediction of axial forces. For the shear forces, the same expressions proposed for the door openings can be adopted with the only exception for the determination of the maximum values of the distribution functions related to the shear actions due to adjacent lintels, $v_{SW7,II,max}$ and $v_{SW7,III,max}$. FE analyses showed in fact that, in case of window openings, the influence due to hold-down stiffness becomes negligible, as shown in Fig. 32, with $v_{u,SW7} = \frac{|V_{SW7}|}{b}$, for values of the hold-down tensile stiffness $k_{h,z,t}$equal to 6609 kN/m and 13247 kN/m.

$$v_{SW7,II,max} = \left[2.5 - 0.1 \bullet \frac{1}{h_{L,l}}\right] \bullet \varepsilon_{v,SW7,II} \bullet \frac{V_{SW7}}{b} \tag{45}$$

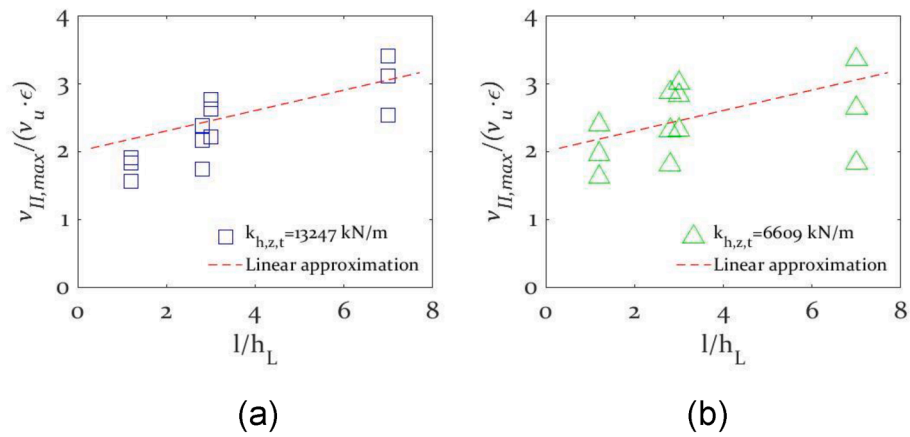

Fig. 35. Normalized representation of $v_{SW8,II,max}$ with $k_{h,z,t}$ equal to (a) 13247 kN/m and (b) 6609 kN/m.

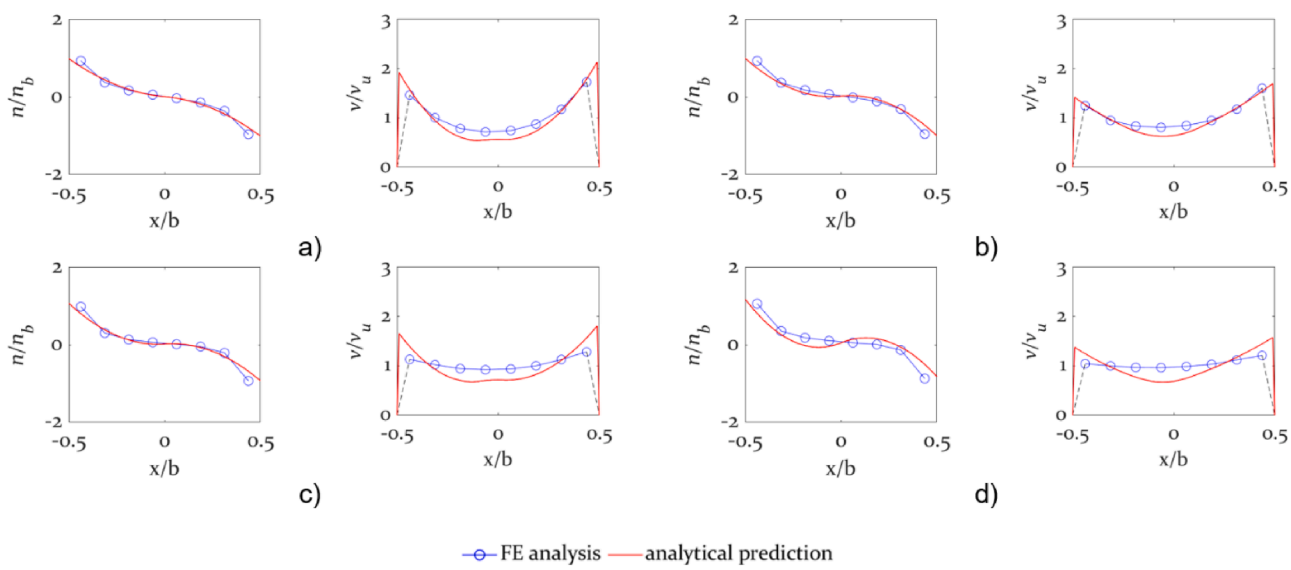

Fig. 36. Distribution of axial and shear internal forces per unit length along section S_{W8}; FE analyses (-o-) and analytical prediction (-): a) l = 2.10 m, h_L = 0.30 m, b = 1.80 m; b) l = 0.90 m, h_L = 0.30 m, b = 1.80 m; c) l = 2.10 m, h_L = 0.75 m, b = 1.80 m; d) l = 0.90 m, h_L = 0.75 m, b = 1.80 m.

$$\text{with} \quad \varepsilon_{v,SW7,II} = \left[1 + \frac{|V_{SW7}|}{|V_{L,l}|} \bullet \frac{h_{L,l}}{b}\right] \tag{46}$$

$$v_{SW7,III,max} = \left[2.5 - 0.1 \bullet \frac{l}{h_{L,r}}\right] \bullet \varepsilon_{v,SW7,III} \bullet \frac{V_{SW7}}{b} \tag{47}$$

$$\text{with} \quad \varepsilon_{v,SW7,III} = \left[1 + \frac{|V_{SW7}|}{|V_{L,r}|} \bullet \frac{h_{L,r}}{b}\right] \tag{48}$$

4.2.5. Section S_{W8}

The distribution of internal forces for the bottom section SW8 of wall segments in CLT shear-walls with window openings is similar to the distribution observed on top sections, as shown in Fig. 33. Similar procedures are hence adopted for the analytical prediction of both axial and shear forces.

As for the top section of wall segments the distribution of axial forces can be expressed by Eq. (51) as the sum of three contributions:

$$n_{z,SW8}(x) = n_{z,SW8,I}(x) + n_{z,SW8,II}(x) + n_{z,SW8,III}(x) \tag{49}$$

The first two contributions, $n_{z,SW8,I}(x)$ and $n_{z,SW8,II}(x)$, take into account the axial stresses due to the adjacent parapets and the external tension reactions R_l and R_r due to hold-down, see Fig. 34.

$$n_{z,SW8,I}(x) = \begin{cases} \dfrac{3 \bullet (V_{P,l} + R_l)}{l_{P,nz,l}^{\,3}} \bullet \left[x + \dfrac{b}{2} - l_{P,nz,l}\right]^2 & for \quad x \le -\dfrac{b}{2} + l_{P,nz,l} \\ 0 \quad for \quad x > -\dfrac{b}{2} + l_{P,nz,l} \end{cases} \tag{50}$$

$$n_{z,SW8,II}(x) = \begin{cases} 0 \; for \quad x < \dfrac{b}{2} - l_{P,nz,r} \\ -\dfrac{3 \bullet (V_{P,r} - R_r)}{l_{P,nz,r}^{\,3}} \bullet \left[x - \dfrac{b}{2} + l_{P,nz,r}\right]^2 & for \quad x \ge \dfrac{b}{2} - l_{P,nz,r} \end{cases} \tag{51}$$

where

$$l_{P,nz,l} = \begin{cases} h_{P,l} & for \quad h_{L,l} \le \dfrac{b}{2} \\ \dfrac{b}{2} & for \quad h_{L,l} > \dfrac{b}{2} \end{cases} \tag{52}$$

$$l_{P,nz,r} = \begin{cases} h_{P,r} & for \quad h_{L,r} \le \dfrac{b}{2} \\ \dfrac{b}{2} & for \quad h_{L,r} > \dfrac{b}{2} \end{cases} \tag{53}$$

The third contribution $n_{SW8,III}(x)$ which is referred to the typical linear distribution of axial forces described in the "beam" theory, is reported in Eq. (56).

$$n_{SW8,III}(x) = \frac{N_{SW8} - V_{P,l} + V_{P,r} - R_l - R_r}{b} - \frac{12 \bullet \left[M_{SW8} - \left(V_{P,l} + R_l + V_{P,r} - R_r \right) \bullet \frac{b}{2} \right]}{b^3} \bullet x \tag{54}$$

The same procedure adopted for the top section of wall segment for door openings is still valid to determine the analytical distribution of internal shear forces. The same expressions proposed for the top section of wall segment for door openings can be adopted with the only exception for the determination of the maximum values, see Fig. 33, of the distribution functions related to the shear actions due to adjacent parapets, $v_{SW8,II,max}$ and $v_{SW8,III,max}$, which can be expressed as:

$$v_{SW8,II,max} = \left[2.0 + 0.15 \bullet \frac{1}{(\mathrm{H} - \mathrm{h_W} - \mathrm{h_{P,l}})} \right] \bullet \varepsilon_{\mathrm{V,SW8,II}} \bullet \frac{\mathrm{V_{SW8}}}{\mathrm{b}} \tag{55}$$

$$\text{with} \quad \varepsilon_{V,SW8,II} = \left[1 + \frac{|V_{SW8}|}{|V_{P,l}|} \bullet \frac{\mathrm{h_{P,l}}}{\mathrm{b}} \right] \tag{56}$$

$$v_{SW8,III,max} = \left[2.0 + 0.15 \bullet \frac{1}{(\mathrm{H} - \mathrm{h_W} - \mathrm{h_{P,r}})} \right] \bullet \varepsilon_{\mathrm{V,SW8,III}} \bullet \frac{\mathrm{V_{SW8}}}{\mathrm{b}} \tag{57}$$

$$\text{with} \quad \varepsilon_{V,SW8,III} = \left[1 + \frac{|V_{SW8}|}{|V_{P,r}|} \bullet \frac{\mathrm{h_{P,r}}}{\mathrm{b}} \right] \tag{58}$$

FE analyses showed in fact that in case of window openings that the influence due to hold-down stiffness becomes negligible, as shown in Fig. 35, with $v_u = \frac{|V_{SW8}|}{b}$ and $h_L = H - h_W - h_{P,r}$ for values of the hold-down tensile stiffness $k_{h,z,t}$equal to 6609 kN/m and 13247 kN/m.

The comparison between numerical models and the equations that approximate them are reported in Fig. 36, where four different geometric configurations are taken into account, as normalized values to $n_{b,SW8} = \frac{6 \bullet |M_{SW8}|}{h_P{}^2}$ and $v_{u,SW8}$.

5. Results analysis and discussion

The results of numerical-analytical parametric study show that the locations of maximum internal forces around openings in CLT walls subjected to lateral loads may vary according to the different analysed parameters.

In terms of different types of anchoring connections (rigid vs. flexible), significant differences were observed, namely the maximum values of axial forces in CLT walls with door openings with rigid anchors were located at the Base-section of Wall Segments (B-WS), whereas the maximum axial force values were located at the End-section of Lintels (E-L) for all cases with flexible anchors. In addition to connection flexibility, the locations of maximum values of axial forces were strongly dependent on the aspect ratio (length over height) of lintels in CLT walls with window openings, namely: i) for slender lintels the maximum values were located at the base of wall segments (B-WS) in walls with rigid anchors and at the end sections of parapets (E-P) in walls with flexible anchors; ii) for wide lintels the maximum values were observed at the bottom corners of the entire panel (C-EP), both for rigid and flexible anchors in majority of cases. In this case the locations of maximum values of shear forces were in all cases located in the corners around the window openings (C-WO) for both, rigid and flexible anchors cases.

The proposed analytical models provide a good correspondence in estimation of internal forces distribution around the openings in CLT walls compared to FE numerical results. A linear distribution of internal forces was observed for axial forces according to "beam theory", while non-linear distribution was identified in most cases for shear forces. It was also demonstrated that the maximum value of internal shear forces per unit length in critical sections cannot be always determined with the well-known expression $v_{max} = \frac{3 \bullet V}{2 \bullet h}$, which is commonly used for CLT beam elements. Specifically, Appendix A3 provides a summary of the analytical expression to determine maximum value of the internal shear forces per unit length for all relevant sections in CLT shear-wall with door and window openings. In addition, maximum shear force ranges are provided for the analysed cases in order to show when maximum shear force values may exceed the commonly used formula for shear force calculation. For instance, maximum shear forces at the lintel edges are 7–33% higher compared to conventional shear force prediction in case of analysed CLT walls with openings, while this range is 1.8–3.2 times higher for the top corner of the door opening of the CLT wall section. In case of CLT walls with window openings, shear force values at the end sections of parapets were 1.13–1.8 times higher compared to the conventional "beam formula" prediction, while this increase range was 1.2–2.1 times higher for wall segments around window openings (see Appendix A3).

The importance of using a correct prediction of shear internal forces in CLT elements (i.e. lintels, parapets and wall segments) is crucial especially when the capacity based designed procedure needs to be applied in order to protect CLT elements from brittle failure modes and to promote the yielding of mechanical anchors.

6. Conclusion

A numerical and analytical investigation on axial and shear internal force distribution in single-storey CLT shear-walls with openings subjected to in-plane lateral loads is presented in this paper. The locations and distribution of maximum values of axial and shear forces in significant wall sections around door and window openings were studied. A parametric finite element (FE) numerical study on 162 cases of single-storey CLT shear-walls with openings, covering a wide range of geometric configurations and anchor connections flexibilities, was performed. The influence of different parameters including door and window opening layouts, lengths and heights of lintels and parapets, wall thicknesses and stiffness levels of anchoring connections (hold-downs and angle brackets) were investigated. Additionally, analytical formulations and mechanical models for determination of axial and shear forces per unit length in wall segments and lintels were proposed. The maximum values of shear and axial forces and their distribution along the wall section were analytically determined and were compared with the results from numerical analyses.

It was demonstrated that the distribution of internal forces in walls with rigid and flexible anchors were considerably different, which implies the importance of adopting a proper discrete CLT connection definition in FE numerical models of CLT walls with openings, as it is currently still widely present in the design practice the aptitude for model a rigid restrain at the bottom of CLT wall segments, which may lead to wrong internal forces distribution around CLT wall openings and wrong locations of maximum internal forces.

The analytical and numerical models provided a good correspondence in the estimation of distribution of internal forces around the CLT openings.

Currently, there are no widespread accepted structural design procedures for the determination of internal forces in walls with openings subjected to in-plane lateral loads. The main outcome of this study

provides closed form analytical expressions to predict maximum values of internal shear and axial forces per unit length and their distribution along the section, for all relevant sections in CLT shear-wall with door and window openings. It was also demonstrated that the maximum value of internal shear forces per unit length in critical sections cannot be determined with currently established expressions, which is also used for CLT beam elements in the structural design practice. Therefore, this study provides original contribution to more correct and precise determination of critical locations and distribution of internal forces in CLT walls with openings subjected to lateral loads, which is of a great importance for the structural design practice and provides in-depth insights of CLT walls with openings internal force distribution behaviour as a foundation for further research explorations of this complex topic.

The obtained outcomes of this numerical-analytical study will serve as a base for the next phase, an experimental campaign on full scale single storey CLT shear-walls with openings. CLT walls with different sizes of door and wall openings, different stiffness levels of anchorage to the foundation and different levels of vertical load will be subjected to in-plane lateral loads with the aim to study in-plane internal force distribution within the CLT panels and failure mechanisms around the wall openings. Experimental results will serve for validation and further extension of numerical and analytical models presented in this paper, leading to a proposal for capacity-based design approach determining the strength of lintel and wall segments in CLT walls with openings in multi-storey CLT buildings.

Declaration of Competing Interest

The authors declare that they have no known competing financial interests or personal relationships that could have appeared to influence the work reported in this paper.

Acknowledgments

CSI Italia srl is deeply acknowledged for providing the software SAP2000 (CSI 2017) used in this work for the implementation of the numerical models. In addition, Igor Gavric gratefully acknowledges receiving funding from programme Horizon 2020 Framework Programme of the European Union; H2020 WIDESPREAD-2-Teaming: (#739574) and the Republic of Slovenia as well as funding received funding from the ForestValue Research Programme which is a transnational research, development and innovation programme jointly funded by national funding organisations within the framework of the ERA-NET Cofund "ForestValue – Innovating Forest based bioeconomy", and ARRS infrastructure program IO-0035.

Appendix A1

A mesh size refinement analysis was performed on a CLT shear-wall with door opening ($l = 2.10$ m, $h_L = 0.75$ m, $b = 1.20$ m, $k_{h,z,t} = 13247$ kN/m) subjected to a lateral displacement equal to 20 mm. The analysis compared the internal forces (bending moment M, shear force V and axial load N) and the distribution of internal forces per unit length in sections SD1 and SD4 for three different sizes of shells element, namely 75.00 mm, 37.50 mm and 18.75 mm. The distribution of internal shear and axial forces for the three different values of mesh size are shown in Figs. A1and A2 for section SD1 and SD4, respectively.

Internal forces, for the three selected mesh size shell element values, and the corresponding discrepancies between the values obtained from the FE numerical model with 18.75 mm mesh size(reference value) and the numerical models are reported in Tables A1 and A2 for sections SD1 and SD4, respectively. The results of this analysis show that the mesh size selection equal to 37.50 mm × 37.50 mm has a good balance between FE model accuracy and the computational effort.

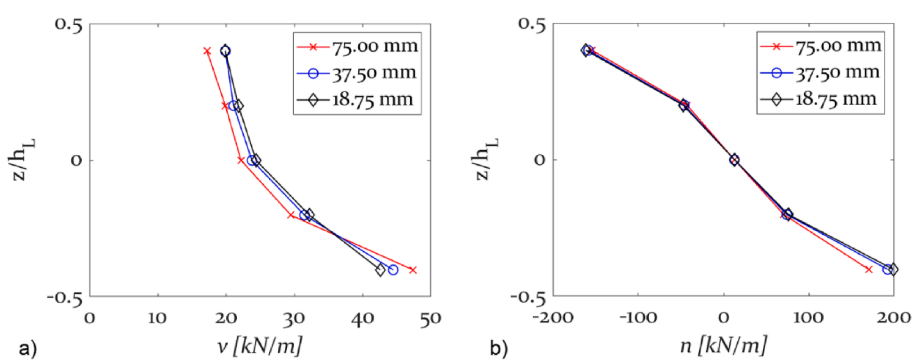

Fig. A1. Section SD1 force per unit length distribution based on FE analyses a) shear force; b) axial force.

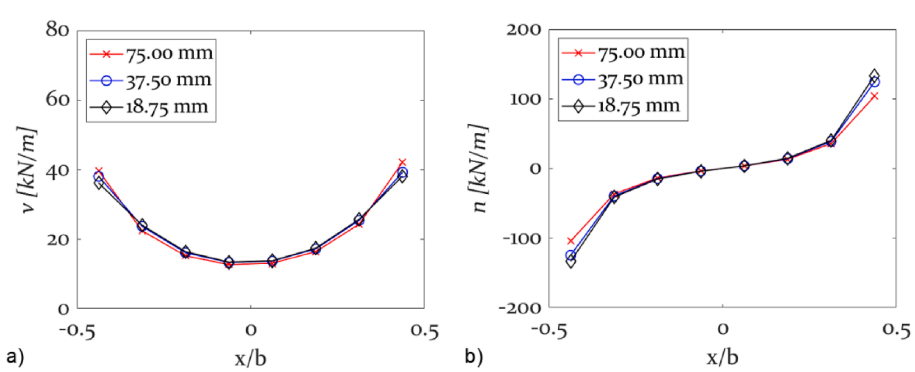

Fig. A2. Section SD4 force per unit length distribution based on FE analyses a) shear force; b) axial force.

Table A1
Section SD1 internal force comparison for three different mesh sizes.

Internal force	Mesh size [mm]		
	75.00	37.50	18.75
N [kN]	13.8 (−1.4%)	13.9 (−0.7%)	14.0
V [kN]	19.5 (−2.0%)	19.8 (−0.5%)	19.9
M [kNm]	20.8 (−0.5%)	20.9 (0.0%)	20.9

Table A2
Section SD4 internal force comparison for three different mesh sizes.

Internal force	Mesh size [mm]		
	75.00	37.50	18.75
N [kN]	0.3 (50.0%)	0.2 (−1.0%)	0.2
V [kN]	26.5 (0.0%)	26.5 (0.0%)	26.5
M [kNm]	30.0 (−2.6%)	30.5 (−1.0%)	30.8

Appendix A2

To determine the exclusion zones, a non-linear elastic analysis was performed on a CLT shear-wall with door opening ($l = 2.10$ m, $h_L = 0.75$ m, $b = 1.20$ m, $k_{h,z,t} = 13247$ kN/m) subjected to a lateral displacement equal to 20 mm. The analysis compared the analytical distribution and the force per unit length obtained by the numerical model. The values of force per unit length at the ends of the column or lintel are reported in Figs. A3 and A4 for section SD1 and SD4, respectively. The analysis shows that the values of the axial force per unit length, at the ends of the column and lintel, significantly deviate from the analytical prediction, which correctly interpolates all other values along the section. For this reason, values of axial and shear force per unit length at the ends of the columns and lintels are not considered in the paper and the exclusion zone of 7.5 cm is considered along all the edges of CLT walls (see Fig. 2).

Appendix A3

A summary of the analytical expression to determine maximum value of the internal shear forces per unit length for all relevant sections in a CLT shear-wall with door and window openings is reported in Tables A3 and A4, respectively.

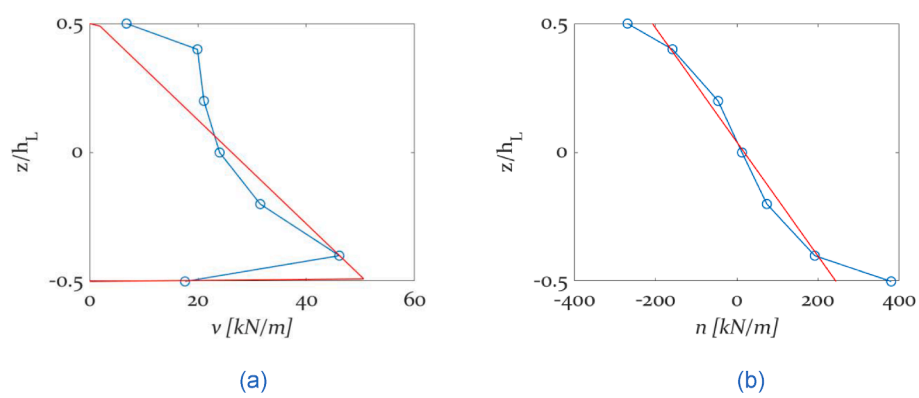

Fig. A3. Section SD1 force per unit length distribution a) shear force; b) axial force (FE analyses (-o-) and analytical (-) prediction).

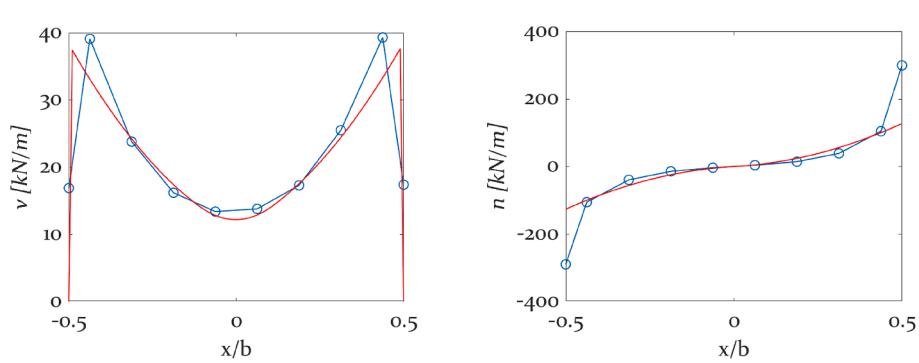

Fig. A4. Section SD4 force per unit length distribution a) shear force; b) axial force (FE analyses (-o-) and analytical (-) prediction).

Table A3
Equations for the maximum values of internal shear forces in shear-wall with door openings.

Section		Distribution of shear forces	Equation for v_{max}	Range of v_{max}
S_{D1}-S_{D3}	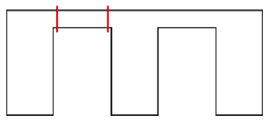	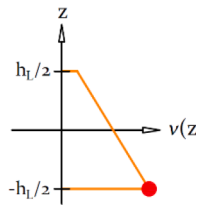	$\left(1.3+0.6\cdot\frac{l}{h_D}\right)\cdot\frac{V_{SD1}}{h_L}$	$[1.6 \div 2.0]\cdot\frac{V_{SD1}}{h_L}$
S_{D2}	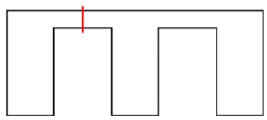	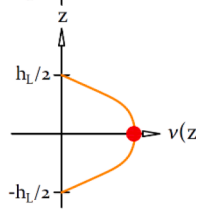	$\frac{3}{2}\cdot\frac{V_{SD2}}{h_L}$	$1.5\cdot\frac{V_{SD2}}{h_L}$
S_{D4}	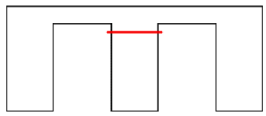	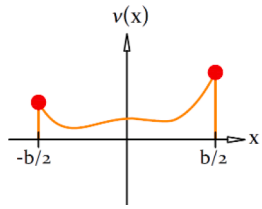	$\left[5.3\cdot\left(\frac{6609}{k_{h,z,t}}\right)^{0.3}-1.5\cdot\frac{l}{h_D}\right]\cdot\varepsilon_{SD4,II}\cdot\frac{V_{SD4}}{b}$ $\left[5.3\cdot\left(\frac{6609}{k_{h,z,t}}\right)^{0.3}-1.5\cdot\frac{l}{h_D}\right]\cdot\varepsilon_{SD4,III}\cdot\frac{V_{SD4}}{b}$	$[2.7 \div 4.8]\cdot\frac{V_{SD4}}{b}$
S_{D5}	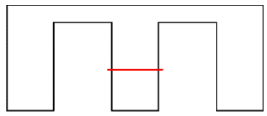	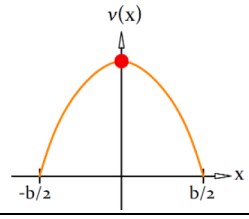	$\frac{3}{2}\cdot\frac{V_{SD5}}{b}$	$1.5\cdot\frac{V_{SD5}}{b}$

Table A4
Equations for the maximum values of internal shear forces in shear-wall with window openings.

Section		Distribution of shear forces	Equation for v_{max}	Range of v_{max}
S_{W1}-S_{W3}	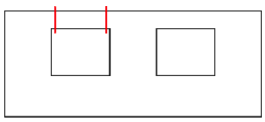	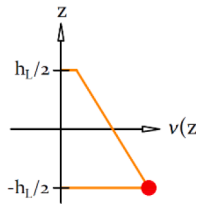	$\left(1.1+0.2\cdot\frac{l}{h_W}\right)\cdot\frac{V_{SW1}}{h_L}$	$[1.3 \div 1.6]\cdot\frac{V_{SW1}}{h_L}$
S_{W2}	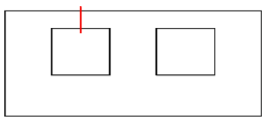	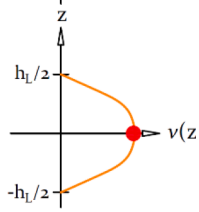	$\frac{3}{2}\cdot\frac{V_{SW2}}{h_L}$	$1.5\cdot\frac{V_{SD2}}{h_L}$
S_{W4}–S_{W6}	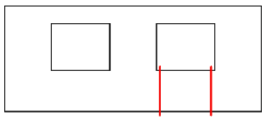	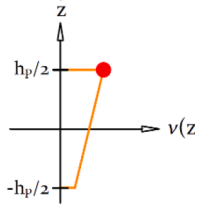	$\left(1.3+0.6\cdot\frac{l}{h_W}\right)\cdot\frac{V_{SW4}}{h_P}$	$[1.7\tilde{A}\cdot 2.7]\cdot\frac{V_{SW4}}{h_P}$
S_{W5}	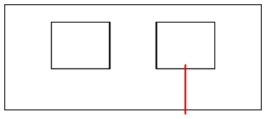	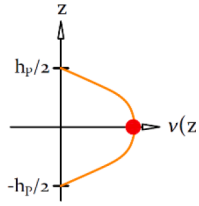	$\frac{3}{2}\cdot\frac{V_{SW5}}{h_P}$	$1.5\cdot\frac{V_{SW5}}{h_P}$
S_{W7}	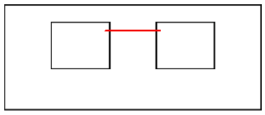	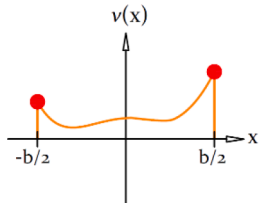	$\left[2.5-0.1\cdot\frac{l}{h_L}\right]\cdot\varepsilon_{SW7,II}\cdot\frac{V_{SW7}}{b}$	$[1.8 \div 2.8]\cdot\frac{V_{SW7}}{b}$
S_{W8}	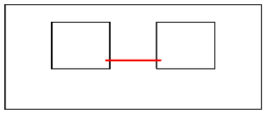	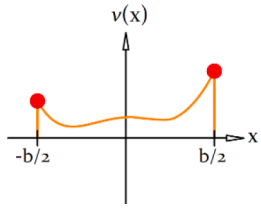	$\left[2.5-0.1\cdot\frac{l}{h_L}\right]\cdot\varepsilon_{SW7,III}\cdot\frac{V_{SW7}}{b}$ $\left[2.0+0.15\cdot\frac{l}{(H-h_W-h_{P,l})}\right]\cdot\varepsilon_{SW8,II}\cdot\frac{V_{SW8}}{b}$ $\left[2.0+0.15\cdot\frac{l}{(H-h_W-h_{P,l})}\right]\cdot\varepsilon_{SW8,III}\cdot\frac{V_{SW8}}{b}$	$[2.2 \div 3.1]\cdot\frac{V_{SW8}}{b}$

The range of maximum values has been determined for the analysed cases, namely: a shear-wall height H equal to 2.70 m, three values of the vertical wall segment's width (b) equal to [1.20; 1.80; 2.40] m, the lintel length (l) and height (h_L) equal to [0.90; 1.50; 2.10] m and [0.30; 0.45; 0.75] m, respectively, and a height of the parapet (h_P) equal to 1.05 m.

References

[1] Awad V, Giresini L, Koshihara M, Puppio ML, Sassu M. Experimental analyses and numerical models of CLT shear walls under cyclic loading. In: Concu G, editors, Wood in Civil Engineering, 2017. https://doi.org/10.5772/65024.

[2] Berg S, Turesson J, Ekevad M, Huber JAJ. Finite element analysis of bending stiffness for cross-laminated timber with varying board width. Wood Mat Sci Eng 2019;14(6):392–403. https://doi.org/10.1080/17480272.2019.1587506.

[3] Bogensperger T, Moosbrugger T, Silly G. Verification of CLT-plates under loads in plane. Italy: Riva del Garda; 2010.

[4] Brandner R, Dietsch P, Dröscher J, Schulte-Wrede M, Kreuzinger H, Sieder M. Cross laminated timber (CLT) diaphragms under shear: test configuration, properties and design. Constr Build Mater 2017;147:312–27. https://doi.org/10.1016/j.conbuildmat.2017.04.153.

[5] Brandner R, Flatscher G, Ringhofer A, Schickhofer G, Thiel A. Cross laminated timber (CLT): overview and development. Eur J Wood Prod 2016;74(3):331–51. https://doi.org/10.1007/s00107-015-0999-5.

[6] Casagrande D, Doudak G, Polastri A. A proposal for the capacity-design at wall- and building-level in light-frame and cross-laminated timber buildings. Bull Earthquake Eng 2019;17(6):3139–67. https://doi.org/10.1007/s10518-019-00578-4.

[7] Casagrande D, Polastri A, Sartori T, Loss C, Chiodega M. Experimental campaign for the mechanical characterization of connection systems in the seismic design of timber buildings. In: Proceedings of the 14th World Conference on Timber Engineering (WCTE), Vienna, Austria, 2016.

[8] Capurso M. Lezioni di scienza delle costruzioni, Pitagora, 1995. ISBN: 8837100477.

[9] Ceccotti A, Lauriola M, Pinna M, Sandhaas C. SOFIE Project - Cyclic Tests on Cross-Laminated Wooden Panels. In: Proceedings of the 9th World Conference on Timber Engineering (WCTE), Portland, USA, 2006.
[10] CSI. SAP 2000. CA, USA: Computers and Structures Inc.; 2017.
[11] Demirci C, Málaga-Chuquitaype C, Macorini L. Seismic drift demands in multi-storey cross-laminated timber buildings. Earthquake Eng Struct Dyn 2018;47(4):1014–31.
[12] Dujic B, Klobcar S, Zarnic R. Influence of Openings on Shear Capacity of Wooden Walls. Bled, Slovenia: paper 40–15-6; 2007.
[13] Dujic B, Klobcar S, Zarnic R. Shear capacity of cross-laminated wooden walls. In: Proceedings of the 10th World Conference on Timber Engineering (WCTE), Miyazaki, Japan, 2008.
[14] ETA 12/0347. European Technical Approval: Cross Laminated Timber (CLT) – Solid wood slab elements to be used as structural elements in buildings, XLAM Dolomiti CLT. Osterreichisches Institut fur Bautechcnik, Vienna, Austria, 2017.
[15] Gavric I, Fragiacomo M, Ceccotti A. Capacity seismic design of X-LAM wall systems based on connection mechanical properties. In: Proceedings of the 46th CIB-W18 Meeting, Paper 46-15-2, Vancouver, Canada, 2013.
[16] Gavric Igor, Fragiacomo Massimo, Ceccotti Ario. Cyclic behaviour of typical metal connectors for cross-laminated (CLT) structures. Mater Struct 2015;48(6):1841–57. https://doi.org/10.1617/s11527-014-0278-7.
[17] Gavric I, Fragiacomo M, Ceccotti A. Cyclic behavior of CLT wall systems: experimental tests and analytical prediction models. J Struct Eng 2015;141(11):04015034. https://doi.org/10.1061/(ASCE)ST.1943-541X.0001246.
[18] Green M, Karsh EJ. The Case for Tall Wood Buildings: How Mass Timber Offers a safe, economical, and Environmentally Friendly Alternative for Tall Building Structures. British Columbia: Creative Commons CC; 2012. p. 1–237.
[19] Izzi Matteo, Casagrande Daniele, Bezzi Stefano, Pasca Dag, Follesa Maurizio, Tomasi Roberto. Seismic behaviour of cross-laminated timber structures: a state-of-the-art review. Eng Struct 2018;170:42–52.
[20] Mestar M, Doudak G, Caola M, Casagrande D. Equivalent-frame model for elastic behaviour of cross-laminated timber walls with openings. In: Proceedings of the Institution of Civil Engineers – Structures and Buildings, 2020. https://doi.org/10.1680/jstbu.19.00057.
[21] Mestar Mohammed, Doudak Ghasan, Polastri Andrea, Casagrande Daniele. Investigating the kinematic modes of CLT shear-walls with openings. Eng Struct 2021;228:111475. https://doi.org/10.1016/j.engstruct.2020.111475.
[22] Pai SGS, Lam F, Haukaas T. Force transfer around openings in cross-laminated timber shear walls. J Struct Eng 2017;143(4):04016215. https://doi.org/10.1061/(ASCE)ST.1943-541X.0001674.
[23] Pauley T, Priestley MJN. Seismic design of reinforced concrete and masonry buildings, Wiley Ed., 1992.
[24] Popovski M, Schneider J, Schweinsteiger M. Lateral load resistance of cross-laminated wood panels. In: Proceedings of the 11th World Conference on Timber Engineering (WCTE), Riva del Garda, Italy, 2010.
[25] Popovski M, Gavric I. Performance of a 2-story CLT house subjected to lateral loads. ASCE J Struct Eng 2016;142(4):E4015006. https://doi.org/10.1061/(ASCE)ST.1943-541X.0001315.
[26] Shahnewaz M, Tannert T, Alam MS, Popovski M. In-plane stiffness of cross-laminated timber panels with openings. Struct Eng Int 2017;27(2):217–23. https://doi.org/10.2749/101686617X14881932436131.
[27] Sustersic I, Fragiacomo M, Dujic B. Seismic analysis of cross-laminated multistory timber buildings using code-prescribed methods: influence of panel size, connection ductility, and schematization. J Struct Eng 2016;146(3):E4015012. https://doi.org/10.1061/(ASCE)ST.1943-541X.0001344.
[28] Tamagnone G, Rinaldin G, Fragiacomo M. Influence of the floor diaphragm on the rocking behavior of CLT walls. J Struct Eng 2020;142(4):04020010, https://doi.org/ 10.1061/(ASCE)ST.1943-541X.0002546.
[29] Timoshenko S. History of strength of materials. McGraw-Hill New; 1953.
[30] Van de Lindt JW, Rosowsky DV, Pang W, Pei S. Performance-based seismic design of midrise woodframe buildings. J Struct Eng 2013;139:1294–302.